

LIDAR Thomson Scattering for Advanced Tokamaks - Final Report

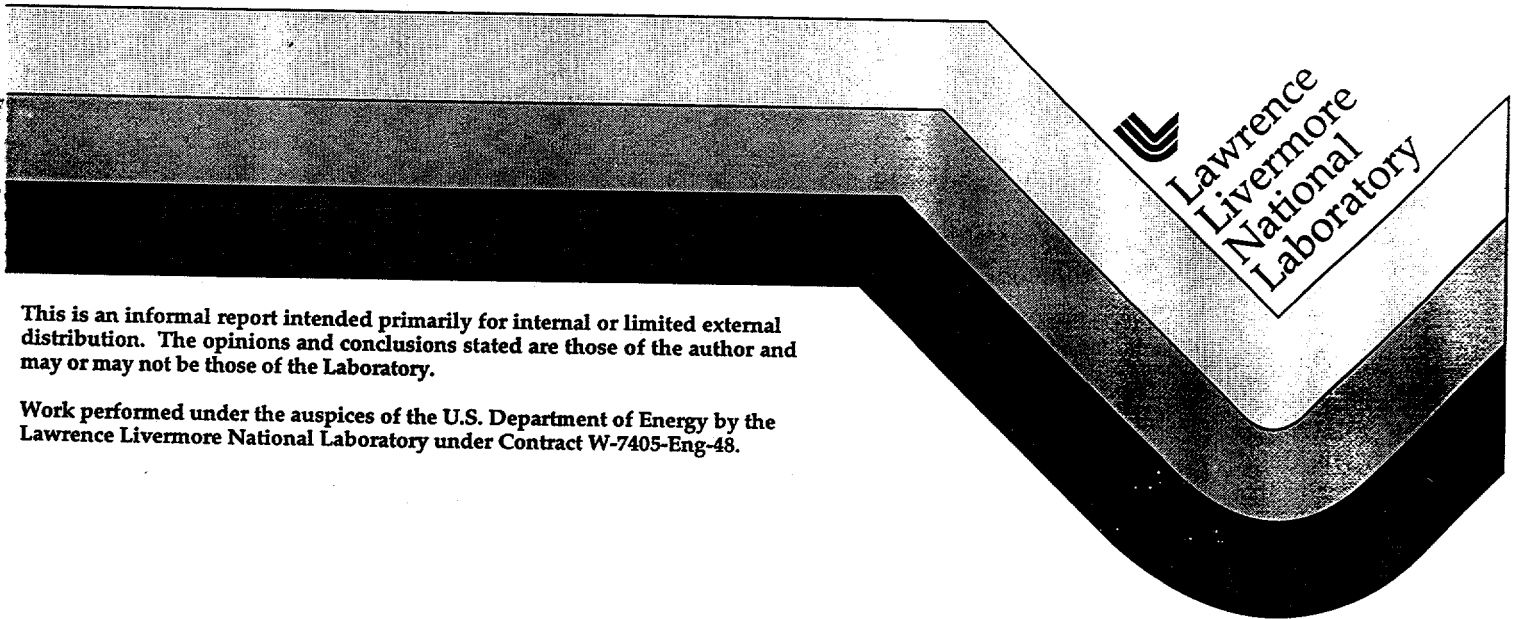
A.W. Molvik, R.A. Lerche, D.G. Nilson, M.D. Perry, E.B. Hooper

RECEIVED

APR 18 1996

OSTI

March 18, 1996



 Lawrence
Livermore
National
Laboratory

This is an informal report intended primarily for internal or limited external distribution. The opinions and conclusions stated are those of the author and may or may not be those of the Laboratory.

Work performed under the auspices of the U.S. Department of Energy by the Lawrence Livermore National Laboratory under Contract W-7405-Eng-48.

DISTRIBUTION OF THIS DOCUMENT IS UNLIMITED *BS*

MASTER

DISCLAIMER

This document was prepared as an account of work sponsored by an agency of the United States Government. Neither the United States Government nor the University of California nor any of their employees, makes any warranty, express or implied, or assumes any legal liability or responsibility for the accuracy, completeness, or usefulness of any information, apparatus, product, or process disclosed, or represents that its use would not infringe privately owned rights. Reference herein to any specific commercial product, process, or service by trade name, trademark, manufacturer, or otherwise, does not necessarily constitute or imply its endorsement, recommendation, or favoring by the United States Government or the University of California. The views and opinions of authors expressed herein do not necessarily state or reflect those of the United States Government or the University of California, and shall not be used for advertising or product endorsement purposes.

This report has been reproduced
directly from the best available copy.

Available to DOE and DOE contractors from the
Office of Scientific and Technical Information
P.O. Box 62, Oak Ridge, TN 37831
Prices available from (615) 576-8401, FTS 626-8401

Available to the public from the
National Technical Information Service
U.S. Department of Commerce
5285 Port Royal Rd.,
Springfield, VA 22161

DISCLAIMER

This report was prepared as an account of work sponsored by an agency of the United States Government. Neither the United States Government nor any agency thereof, nor any of their employees, makes any warranty, express or implied, or assumes any legal liability or responsibility for the accuracy, completeness, or usefulness of any information, apparatus, product, or process disclosed, or represents that its use would not infringe privately owned rights. Reference herein to any specific commercial product, process, or service by trade name, trademark, manufacturer, or otherwise does not necessarily constitute or imply its endorsement, recommendation, or favoring by the United States Government or any agency thereof. The views and opinions of authors expressed herein do not necessarily state or reflect those of the United States Government or any agency thereof.

DISCLAIMER

Portions of this document may be illegible in electronic image products. Images are produced from the best available original document.

UCRL-ID-123434

**LIDAR Thomson scattering for advanced tokamaks –
Final report**

A. W. Molvik, R. A. Lerche, D. G. Nilson, M. D. Perry, and E. B. Hooper

March 18, 1996

LIDAR Thomson scattering for advanced tokamaks – Final Report

A. W. Molvik, R. A. Lerche, D. G. Nilson, M. D. Perry, and E. B. Hooper

Summary

The LIDAR Thomson Scattering for Advanced Tokamaks project made a valuable contribution by combining LLNL expertise from the MFE Program: tokamak design and diagnostics, and the ICF Program and Physics Dept.: short-pulse lasers and fast streak cameras. This multidisciplinary group evaluated issues involved in achieving a factor of 20 higher high spatial resolution (to as small as 2-3 mm) from the present state of the art in LIDAR Thomson scattering, and developed conceptual designs to apply LIDAR Thomson scattering to three tokamaks: Upgraded divertor measurements in the existing DIII-D tokamak; Both core and divertor LIDAR Thomson scattering in the proposed (now cancelled) TPX; and core, edge, and divertor LIDAR Thomson scattering on the presently planned International Tokamak Experimental Reactor, ITER.

Other issues were evaluated in addition to the time response required for a few millimeter spatial resolution. These include the optimum wavelength, 100 Hz operation of the laser and detectors, minimizing stray light – always the Achilles heel of Thomson scattering, and time dispersion in optics that could prevent good spatial resolution.

Innovative features of our work included: custom short pulsed laser concepts to meet specific requirements, use of a prism spectrometer to maintain a constant optical path length for high temporal and spatial resolution, the concept of a laser focus outside the plasma to ionize gas and form an external fiducial to use in locating the plasma edge as well as to spread the laser energy over a large enough area of the inner wall to avoid laser ablation of wall material, an improved concept for cleaning windows between shots by means of laser ablation, and the identification of a new physics issue – nonlinear effects near a laser focus which could perturb the plasma density and temperature that are to be measured.

I. Introduction

LIDAR (Light Detection And Ranging) Thomson scattering was first developed for the JET (Joint European Torus) Tokamak,¹ where it measures the electron density and temperature with high reliability, Fig. 1. The electron density is proportional to the flux of scattered photons, and the velocity distribution or temperature of electrons can be inferred from the Doppler shifted spectral distribution of scattered photons. LIDAR is the laser analog to RADAR: measuring the time of flight of back-scattered photons determines the axial location of the scattering. On JET, features smaller than the 10 cm (4") length of the laser pulse could not be measured, and the laser could fire only once every 2 sec. Advanced tokamaks require measuring 3 mm (1/8") features 100 times per sec.

Utilizing 3 recent developments in laser technology,² laser pulse lengths of a few millimeters, firing 10 to 100 times per second, are possible. (1) Chirped-Pulse Amplification allows high energy lasers to achieve pulse durations of less than a picosecond (a millionth of a millionth of a second), Fig. 2. These pulses are less than 0.3 mm (1/80") long. (2) Laser diodes inject the precise wavelength of light needed for efficiently pumping lasers. Conventional flashlamp pumping injects a wide range of wavelengths of light, most of which is wasted as heat, thus requiring more cooling. (3) Microchannel cooling removes heat from the laser more uniformly and quickly. Repetitive measurements 100 times per second place special requirements on not

only lasers, but also on streak cameras, and CCD cameras. Fast decay phosphors and low fractional drain image intensifiers are necessary for the streak camera. Readout rates of CCD cameras have reached 400 frames per second, but at high noise levels. Acceptable noise levels at 100 frames per second are expected with a few years. LLNL expertise in picosecond laser technology and fast streak camera detectors makes ≤ 1 cm resolution LIDAR Thomson scattering possible. LIDAR Thomson scattering provided an unusual opportunity for a collaborative effort between the ICF and MFE programs.

LIDAR Thomson scattering (TS) has several advantages over conventional TS. Diagnostic access is very limited in modern tokamaks, particularly in the divertor region, see Fig. 3 for TPX. This illustrates that conventional Thomson scattering requires 2-3 ports in the same plane for the laser input, dump and the viewing system. Conventional TS also has the disadvantage that it cannot follow radial shifts in the plasma minor axis, unlike LIDAR TS for which both the laser and the viewing can lie along the horizontal midplane, so that data is always acquired from the plasma axis, and its position and motion are measured. In DIII-D, Fig. 4, a laser can access the divertor from the strike point to the x-point, however, the conventional TS viewing system is blocked by structure except near the x-point. LIDAR TS requires only a single port. Midplane LIDAR, as in JET [1], would be straight forward in any tokamak. Divertor LIDAR Thomson scattering, between the strike point and the x-point, may be possible through 3" diameter V1 ports in DIII-D using a periscope system to jog the laser and viewing sideways from V1 to the divertor, Fig. 5.

Divertor simulation codes, which are essential for scaling up to machines like ITER, need diagnostic data to benchmark. At present, electron temperature and density data exist only near the X-point and the strike point of divertors. Conventional TS divertor designs measure across the divertor, somewhere between the strike point and the x-point. LIDAR TS can do the same measurement more easily. While measurements along this line delivers useful information, not previously available, measurements along a line between the strike point and the x-point would be much more useful in fully diagnosing the decay of the electron temperature towards the strike plate and towards the recombination regions of gaseous divertors which can move towards and away from the x-point due to variation of the gas feed rate. Such measurements, if possible at all, are only possible with LIDAR TS. The major difficulties will be in perforating the strike plate without unacceptable degradation of the power handling capability, and measuring scattered light in the presence of intense emission from a gaseous divertor. The short-pulse laser, delivering the order of a Joule in ~ 10 ps rather than several ns, increases the signal-to-noise ratio significantly in the presence of intense plasma light emission.

Steep temperature and density gradients with 1 cm scale lengths are observed near the edge of tokamak plasmas, particularly during H and VH modes, requiring diagnostics with good spatial resolution. Conventional Thomson scattering requires additional sets of channels of viewing, spectrometer and detector to provide good spatial resolution. LIDAR requires one set with time resolution.

We have identified several areas of the design that are critical to measuring features as small as the few mm length of the laser pulse. (1) The scattering angle must be very near 180° with large diameter laser beams, because the apparent thickness of the thin disk of light increases when viewed at an angle towards the side. (2) Every ray of light from a point in the plasma must have the same optical length, within a few mm, to the detector. This is automatically achieved with prism spectrometers and lens train viewing systems and is easily achieved with filter spectrometers. But a phase correction plate would need to be developed for grating spectrometers and fiber optics would need to use gradient index techniques to achieve the same optical path length for every angle of light ray. (3) Low electron temperatures cannot be measured with very short pulses ($\ll 1$ ps) because

the shorter the laser pulse duration, the wider the spread in wavelength of the laser, but the electron temperature is inferred from the spread in wavelength of the scattered light.

We have also identified a new physics issue: to determine the power density limit for Thomson scattering, above which it cannot measure electron temperatures because non-linear effects create a significant axial electron velocity exceeding the thermal velocity, or the density because non-linear effects perturb that. Such problem will occur only at very high power densities, which occur only near the focus of a short pulse laser. We evaluated effects that could produce these limitations, and designed an experiment to test the limits.

We conclude that LIDAR Thomson scattering is viable both in the core of a tokamak and also in the divertor where it could measure density and temperature from the core to near the wall.

The organization of this report discusses general design issues in the next section. These include the time response necessary to achieve the desired, spatial resolution, the optimum wavelength and laser material, issues and solutions with 100 Hz operation, minimizing stray light detection – both from laser prepulse as well as from the main pulse, time dispersion in optics that could prevent achieving the required spatial resolution, and a concept for window cleaning between shots by laser ablation. The third section discusses the application of LIDAR Thomson scattering to three specific tokamaks: the existing DIII-D, and the proposed TPX and ITER. Finally, we discuss a new physics issue for focused short-pulse lasers and the planning for an experimental test of this issue and demonstration of few millimeter spatial resolution.

Mention of a company or product does not imply endorsement by either the authors or by LLNL. No products were evaluated during this work.

2. General design issues

2.1. Time response and spatial resolution

The total time response can be determined by several elements: the laser pulse length τ_l , the detector response time τ_d , and the recorder response time τ_r . These add in quadrature. The spatial resolution gains a factor of two, because the light traverses the path twice – once from the laser to the plasma, then scattered from the plasma back to the detector. The spatial resolution δl is then given by

$$\delta l = \left(\tau_l^2 + \tau_d^2 + \tau_r^2 \right)^{1/2} c / 2$$

2.2. Wavelength and laser type

We found that a 1.06 μm wavelength, frequency doubled to 0.53 μm (with 0.8 μm , frequency doubled to 0.4 μm preferable for very high electron temperatures³), was the preferred wavelength, as discussed below. Initial considerations indicated that Nd:YAG lasers were appropriate, subsequent designs of possible laser architectures indicated that other amplifier media might be preferable.

The choice of LIDAR Thomson scattering wavelength is detailed in Table 1. To summarize: the selected wavelength of 0.53 μm (green) is near the minimum of plasma

and wall radiation (plasma radiation increases towards the ultraviolet, and radiation from walls at a few hundred degrees increases towards the infrared). Available photo-cathode quantum efficiencies are maximum near 0.4-0.5 μm and have much better long term stability than do S-1 photocathodes at 1.06 μm . Finally, the prepulse energy is reduced, and most of the prepulse remaining will be at 1.06 μm , for which the photo-cathode (S-20 or RCA-111) sensitivity is down by several orders of magnitude. Subsequent studies have indicated that for the core, it might be preferable to measure the scattered spectrum over the maximum possible range, so that a laser at the blue or red end of the visible range, i.e., 400 or 800 nm, would allow a spectrograph with associated windows and lenses to function over several hundred nm between 400 and 800 nm.³

Table 1. Advantages and disadvantages of the fundamental 1.06 μm wavelength versus its harmonics.

<u>Wavelength</u>	<u>Advantages</u>	<u>Disadvantages</u>
1.06 μm	<ul style="list-style-type: none"> • Twice power of 0.53μm laser • 4-5 times higher damage threshold • Better beam quality 	<ul style="list-style-type: none"> • Background light radiated by hot walls is significant • Streak camera S-1 cathode has ~0.4% efficiency of S-20 @ .53μm • Photocathode sensitivity decays in time • Prepulse greater $\sim 10^{-3}$
0.53 μm	<ul style="list-style-type: none"> • Probably near minimum of plasma and wall radiation • Streak camera S-20 cathode 13% efficiency (250\times more efficient at 0.53 μm than S-1 at 1.06 μm. Type 111 $\sim 400\times$ better) • Photocathode sensitivity stable • Prepulse lower ($\sim 10^{-6}$) • Prepulse mostly 1μ, can reject with filter, double grating, photo-cathode 	<ul style="list-style-type: none"> • Lower energy: $\times 0.3-0.5$ of 1μm • Lower damage threshold • Poorer beam quality
0.35 μm	<ul style="list-style-type: none"> • Streak camera S-20 cathode has $\geq 20\%$ efficiency 0.35-0.46 μm 	<ul style="list-style-type: none"> • More plasma light • Poorer window transmission, except for selected materials • Lower conversion efficiency

A pulse length of 10-40 ps is required for 0.25-1.0 cm spatial resolution. The shortest pulse length feasible from a chirped Nd:YAG laser is 10 ps. This is restricted by the narrow bandwidth of Nd:YAG.

A narrow bandwidth is required of $\ll 3.0$ nm in a divertor, which corresponds to the full width of the Doppler broadening of the Thomson scattered spectrum from 0.5 eV electrons. Nd:YAG has bandwidth of 0.42 nm, and a chirp width ≈ 0.15 nm, which meets requirements of not restricting the minimum electron temperature. Nd:Glass has a bandwidth of 3.2 nm which is marginal. Ti:Sapphire has a bandwidth of 16.4 nm which, if filled, is unsatisfactory for divertor applications, but might be satisfactory for core Thomson scattering.

Nd:YAG can be flash lamp pumped for lower near term cost. Diode pumps allow much higher repetition rate, to the order of 10 kHz, but the cost is 5× that of flash lamps today. Price drops are expected soon, so diode pumping may be affordable for TPX and ITER. Nd:YAG has high gain, so it needs fewer amplifier stages than glass or Ti:Sapphire. The thermal conductivity is high enough to cool at 10 Hz pulse rate, but thermal lensing stability requires steady repetition rate operation of the laser all day.

Low prepulse energy is important so that the tokamak is not filled with light that will return through the viewing system increasing the background light level and raising the measurable density threshold.

The damage threshold for mirrors and lenses allows ~1J in a 2.1 cm diameter beam at a pulse length of 40 ps. The damage threshold scales with (pulse duration)^{0.5} for pulses longer than about 10 ps, and levels out below that duration.⁴

2.3. 100 Hz operation

Two laser concepts, which could be built today, are (1) 0.2-10 ps pulse length at 800 nm, 0.6 J, 100 Hz with a diode pumped final stage, costing 2.2 M\$ (1994), Fig. 6; (2) If higher energy is needed, 2-20 ps pulse length at 1053 nm, 6 J, 3-5 Hz flashlamp pumped, costing 1.5 M\$ (1994), Fig. 7. The cost of diode pumping is dropping rapidly; higher energy, more rapidly pulsed lasers will be affordable within a few years. Either laser can be frequency doubled with an efficiency near 50%. The 10 ps laser beam needs to be transported with mirror optics, with the integrated window thickness kept below 1 cm to avoid beam breakup. For this reason, pulse compression and harmonic doubling are performed as close as possible to the plasma.

The LLNL Laser Program Ultrafast Streak Camera provides time resolution approaching 10 ps, Fig. 8,⁵ which is compatible with spatial resolution of 1.5 mm if limited only by the streak camera. Cylindrical electrostatic focusing, Fig. 9, of a 1.2 mm wide input slit produces an output resolution of ~300 μm corresponding to 120 pixels in time. An S-20 photocathode provides a high quantum efficiency at either 400 or 527 nm.⁶ This type of instrument is essential to achieving time resolution below 40 ps. The sweep circuitry and phosphor persistence times will need to be tested to assure 100 Hz operation of the streak camera. Photomultiplier tubes followed by digital recorders become an option if the time response is relaxed to the order of 150 ps, and are less subject to repetition rate issues.

CCD detector readout of a streak camera is accomplished more rapidly by "binning" CCD columns together. Binning means to add 2 or more rows or columns of pixels together before reading out. JET measures from 0.2-14 keV with 6 channels, so a comparable number of channels should suffice for the 0.5-50 eV range and the reduction in wavelength resolution should not be detrimental. A weakness of the binning technique has been "blooming", where the addition of many nearly saturated CCD pixels into one pixel results in exceeding the full well capacity of that pixel and the excess charge spills over into adjacent pixels. The recent introduction of anti-blooming CCDs reduces this problem by a factor of 1000. An alternative method of reading several channels from a streak camera, each maintaining a high time resolution, has been used in the past by L-Division. A set of 4 to 10 fiber optic bundles fanned out from the streak camera output, each to a 512 or 1024 channel linear Reticon detecting a particular spectral channel. A rough cost estimate from Fiberguide is a few tens of k\$ for the fiber array, which is comparable to a CCD camera, even without the Reticons and associated electronics.

The state of the art in CCD readout rate is 400 frame/s with a 512×512 CCD with 9-10 bits resolution and a 100-150 electron noise floor achieved at LLNL. Higher resolution, of at least 12 bits, is desired along with lower noise. Commercial products from, for example Princeton Instruments, have achieved 160 frames/s with a 576×384 binned CCD with a 50 electron noise floor, for 75 frames/s with a 27 electron noise floor.

2.4. Minimizing stray light

A critical issue in all Thomson scattering systems is the minimization of stray laser light that scatters off of optics and structure rather than off of electrons. The Thomson scattered photon flux is typically about 13 orders of magnitude below the incident photon flux. The stray light problem in the divertor region of DIII-D is even more severe than usual because the viewing system and laser must both fit within a 7.9 cm diameter by 165 cm long tube (V1), then jog sideways 22 cm with a periscope-like system to access the radiative divertor, Figs. 4,5.

Possible causes of scattered light include stray laser light, prepulse laser light, carbon films and dust within the laser beam, and damaged optics. It is generally necessary to employ every possible technique to reduce stray light, both its production, and its detection.

Carbon, boron, or beryllium films and dust are problems because all plasma facing walls in modern coated with one of these low-z materials in order to minimize the cooling effect of high-z impurities in the plasma. These are undesirable on optics and are minimized by (1) Locating the LIDAR system at the top rather than the bottom divertor although the bottom position is shown in Figs. 4 and 5., (2) Closing a shutter between the plasma and the nearest mirror during discharge cleaning, (3) Using an electric field to sweep charged dust away from optics, (4) Refinement of JET laser ablative cleaning to provide routine cleaning before each shot.

Damage thresholds determine the maximum laser power through a given size window or mirror. We will need to experimentally measure the damage threshold for ablative cleaning to determine whether cleaning is possible without damage to the optical surfaces of mirrors or windows, which could cause unacceptable levels of back-scattered laser light. We also need to determine the arrival rate of dust and film deposits, to determine whether sufficient accumulation will occur in the 100 ms between full power shots to cause damage.

Other techniques to be employed include minimization of the laser prepulse, removal of 1.06 μm light, and the usual care with laser windows, baffles, and laser beam confinement tube, accentuated by the confined 3 1/8" diameter tube that laser and viewing system must share for the DIII-D divertor.

2.4.1 Prepulse

Prepulse light is typically emitted by lasers before the main pulse. It is a problem because if it is sufficiently early, it can reflect off the far wall (laser beam dump) and arrive at detectors at the same time as the desired signal. Nd:YAG appears to be marginal in this respect, with a prepulse fraction of 10^{-4} - 10^{-3} (10^{-5} with effort) at 1.06 μm , which is reduced further to 10^{-7} - 10^{-6} at 0.53 μm after the harmonic converter. The prepulse at 0.532 μm is the major issue, since other techniques can filter out the 1.06 μm component. Nd:Glass is superior in this attribute with prepulse levels of 10^{-12} at 0.53 μm and 10^{-6} at 1.06 μm .

A harmonic separator at 45° to the laser beam, after the harmonic converter, will transmit 90% of the 0.532 μm light, and reflect 99.7% of the 1.064 μm light to a dump. The streak camera photo-cathode (S-20 or 111) quantum efficiency is down from its value at 0.532 μm by a factor of 0.0032 at 1.064 μm.

Laser light will be dumped on the inner wall. If the wall is rough graphite, with a reflectivity ≤0.2, at a distance of 1.4 m from 18 – 0.7 cm viewing windows, a maximum of 6×10^{-6} of the laser light will be scattered back into the viewing system. A polished graphite mirror on the carbon inner wall would reflect the light to the bottom carbon wall, returning 3×10^{-7} to the viewing system without a dump. The total scattered light fraction at 1.06 μm from laser prepulse is

(Prepulse fraction)(Harmonic separator)(Photocathode relative to 0.53μm)(Dump reflection)(Viewing system solid angle)(Viewing system transmission)

$$(10^{-3} \text{ to } 10^{-5})(0.003)(.0032)(6 \times 10^{-6})(0.015)(0.2) = 1.7 \times 10^{-16} \text{ to } 1.7 \times 10^{-18} .$$

The total scattered light fraction at 0.532 μm from laser prepulse is

$$(10^{-6} \text{ to } 10^{-7})(1.0)(1.0)(6 \times 10^{-6})(0.015)(0.2) = 1.8 \times 10^{-14} \text{ to } 1.8 \times 10^{-15}$$

For a 0.4 J laser with 1.1×10^{18} photons, 2 to 170 photons at 1.06 μm, and 2×10^3 to 2×10^4 photons at 0.532 μm are available to create photoelectrons at the photo-cathode. Since this number needs to be small compared with a signal of ~1000 photons, further reductions are necessary. Installation of a beam dump that reflects $< 10^{-2}$ of the photons incident on the bottom wall, coupled with a clean graphite mirror on the inner wall that back-scatters $< 10^{-2}$, would reduce the 1.06 μm light to an insignificant level, and nearly take care of the 0.532 μm light which would have 0.2 to 20 prepulse photons arriving at the photo-cathode. Prepulse reduction to 10^{-8} , if not too costly, would be helpful on DIII-D.

If we had enough signal to restrict the spectrometer resolution to ≤1.5 nm (comparable to the laser width), then we could place a mechanical block at the focus of the spectrometer (If the streak camera has a fiber-optic face plate or we use an additional lens to couple it to the spectrometer). A similar block could be installed between the streak camera and the mcp intensifier. This would ameliorate stray laser light causing saturation of the mcp which can result in a blooming-like effect called veiling. Such laser-line blocks should be able to reduce the laser signal a factor of 10-1000 (depending on how small we can make the spectrometer input slit), which combined with care in minimizing prepulse in the first place, gives an acceptable number of prepulse photons to the streak camera. (This is not feasible with a 0.4 J laser that fits the space and budget constraints on DIII-D.)

2.4.2. Stray light from the main laser pulse

Measuring electron temperatures in the 0.5 – 50 eV range requires that each spectrometer channel have a resolution in the range of 1.5-15 nm half-widths, which unfortunately eliminates some very effective techniques for reducing stray laser light such as the mechanical notch filter discussed in the preceding section. Optical notch filters can attenuate a laser line by 6 orders of magnitude, but they have a bandpass of 10 nm which would prevent temperature measurements below about 25 eV. Even if used off-center, the edge width is 4 nm, which would prevent temperature measurement below about 5 eV.

Rejecting prepulse light by gating the streak camera or detectors also is of limited effectiveness if optics are close to the plasma. Three components of a streak camera are capable of being gated: the photo-cathode, the deflection plates, and the mcp intensifier. The following data were supplied verbally by a Hadland representative (William Cieslik) at the CLEO94 Conference as characteristic of their faster streak cameras. The photo-cathode can be gated in ~100 ns with extinction ratios of 10^6 – 10^7 . The deflection plates can be gated in less than 1 ns with extinction ratio of 10^3 . Finally, the mcp can be gated with a 400 ns rise plus fall time. Faster gating is achievable.⁷ Comparing these with the time of flight between the final mirror in a DIII-D divertor TS and the divertor strike point (~6 cm distance) of 200 ps, or 400 ps to reflect back, we see that gating does not help to reduce scattered light from this source. However, if the laser light reflects off of a polished carbon reflector on the inner wall of DIII-D, to a beam dump on the bottom wall, about 2.8 m below the top wall, returning light will be delayed by ~8–16 ns, which is enough time to gate the deflection plates to off. On the other hand, the core LIDAR TS in ITER has ~3 m between the final mirror and the plasma, giving a more reasonable 18 ns in which to gate-on detectors to discriminate against laser light scattered by the mirror. The Nova laser facility operates with a similar distance between the final focusing lens and the target, and routinely shares that lens between the laser and back-scatter diagnostics – although none are as sensitive to stray light as Thomson scattering.

The scattered light from main pulse can be estimated. High quality optical surfaces will scatter 10^4 of the laser light.⁸ A possible geometry of the radiative divertor in DIII-D is shown in Fig. 4. The laser beam does not strike a wall until it reaches the inner wall at a distance of 1.8 m from the final mirror. Scattered light from the mirror must reflect at least once from the tube to reach the divertor channel to either side, we assume a reflectivity of 0.1 for the blackened walls of the tube and for the carbon tiles that constitute all plasma facing surfaces in DIII-D. The lenses of the viewing system must be close to the end of the viewing tube (which is completely separate from the laser tube so no light can scatter directly into the viewing system), so that the entire laser beam can be viewed from the strike point on the floor of the divertor channel to the x-point 30 cm above. This is accomplished without including the divertor channel walls in the field of view by using a cylindrical lens to distort the viewed region from circular to fan shaped. Viewing windows are displaced azimuthally to both sides of the laser (out of the plane of the paper in Figs. 4,5) to provide a view along the divertor channel, rather than across it. Stray light reflected by the divertor channel will reach the viewing window, but will be out of the field of view, so will be absorbed by multiple bounces along the tube, leaving only the fraction, 10^{-3} , that scatters off the viewing window. We then have a scattered light signal of

Scattered fraction = (Window scattering)(Tube reflectivity)(Tile reflectivity)(viewing solid angle from tile)(Window scattering)(Fiber optic solid angle)

$$\begin{aligned} \text{Scattered photons} &= (10^{-4})(10^{-1})(10^{-1})(1.25\text{cm}/10\text{cm})^2(10^{-4})(0.15\text{mm}/(2*15\text{mm}))^2 \\ &= 3.9 \times 10^{-17} \end{aligned}$$

With a 0.4 J laser (1.1×10^{18} photons), we have 43 photons in the viewing system. When multiplied by the transmission (0.20) and the quantum efficiency of the photocathode (0.21), we still are left with 1.8 photoelectrons, which is much smaller than the signal that we expect (Section 3.2.1). A critical issue then is measuring the scattered light from the quality of optical surfaces that we expect to be able to maintain in DIII-D to ensure that 10^{-4} scattered fraction is achievable, and also obtain more accurate measurements of tube and tile reflectivities.

2.5. Time dispersion in optics

Time dispersion in optics reduces spatial resolution. Control involves selection of the proper type of fiber optic bundles, and keeping all the lengths equal. Tests in Y-Division have shown that little time dispersion occurs with graded index 50 μm core fibers of up to 100 feet in length using monochromatic laser light. We will need bundles of such fibers for the viewing system. Development is required to achieve high packing fractions of acceptance area in the bundles. However, a gradient index fiber optic is still subject to chromatic time dispersion, which is 460 ps/nm-km for a particular design. This limits individual channel widths to ≤ 3.5 nm for 40 ps response from a 25 m long fiber. Channel to channel time shifts can be corrected.

Grating spectrometers introduce time dispersion, yielding a spatial resolution of the order of the grating diameter, indeed this feature of gratings is essential to short pulse lasers for stretching the chirped beam in time before amplification, then recompressing the beam in time after amplification. A fiber-optic step plate, Fig. 5, can equalize optical path lengths to within the required spatial resolution if inserted before the grating in a spectrometer. This must be installed in a collimated light path, and carefully aligned with the fiber axis parallel to the light path. We cannot use the usual Czerny-Turner spectrograph configuration because the reflected rays from the grating nearly retrace their path, so there is no place to install the fiber-optic step plate. A transmission grating (such as those made by Kaiser Optical Systems, Inc.) with lens collimation appears to be easier to use with the step plate, and provides a higher efficiency.

A prism spectrometer has equal path lengths for every ray (before spectral dispersion). However, a prism provides less spectral dispersion than a grating, and is not linear – although lack of linearity is only a minor inconvenience. High spectral dispersion is needed primarily to allow wider input slit width, at a given spectral resolution, which allows a larger fiber-optic bundle to gather more signal. High spectral dispersion also yields a better match to the streak and CCD cameras, and can be achieved with prism spectrometers by lens coupling to the detector. A filter spectrometer looks difficult in the divertor region, due to requirements of high spectral resolution (15-150 \AA half widths must be resolved) but is reasonable for the core where electron temperatures exceeding 1 keV yield spectral half widths in excess of 300 \AA .

2.6. Routine window cleaning by laser ablation

Laser ablation cleaning is used periodically on JET to remove deposits from the viewing windows.⁹ The laser input window is self-cleaning. We considered a scenario that would allow cleaning to be done between tokamak pulses. The laser pulses continuously (all day) to maintain constant thermal lensing. We rotate a wave plate/polarizer plate in 1.06 μ beam path between DIII-D shots to attenuate the laser beam to ~ 0.05 power, and reflect the remainder to a beam dump during discharge cleaning. Then between shots, the beam is reflected to beam splitters and 0.5 cm fused silica fiber optic bundles that transmit ~ 0.05 laser power through each viewing window and mirror. Some of the requirements and features are:

- Fiber optic bundles have different lengths so laser beams do not coincide in time.
- Paired bundles either side of viewing fibers illuminate entire mirrors
- Lens couple and shape bundles to illuminate mirror but not adjacent structure
- Extra bundles could be used to clean other windows on DIII-D
- Interlocked shutter on diagnostic fibers to block stray cleaning light from streak camera
- Interlocked shutter between laser and cleaning fibers to keep stray laser light out of viewing system

Some issues are:

- Can LIDAR be on top to minimize dust accumulation?
- How many dust particles accumulate in 100 ms between full energy shots? These can cause damage to windows mirrors.

- How far below damage threshold must cleaning pulses be to avoid damage in presence of carbon dust or film.
- Do we need to continuously monitor damage on mirrors and windows?

3. Application to specific devices

3.1. DIII-D divertor

The requirements for LIDAR Thomson scattering in the DIII-D radiative divertor, Figs. 4,5, and in the midplane and divertor of TPX, Fig. 3, are summarized in Table 2, and discussed below and in the next section.

Table 2. LIDAR Thomson Scattering requirements for DIII-D and TPX

Parameter	DIII-D Radiative Divertor	TPX Midplane	TPX Divertor
Machine requirements		[Unofficial]	[Unofficial]
Date needed	1996	2000	>2000
T_e	0.5-50 eV	0.2-20 keV ?	0.5-50 eV
$(\delta\lambda)$	$\pm 1.5-15$ nm	$\pm 30-300$ nm	$\pm 1.5-15$ nm
n_e (m^{-3})	$10^{19} - 10^{21}$	$10^{19} - 2 \times 10^{20}$	$10^{19} - 10^{21}$
Spatial resolution	0.2-1 cm	1-2 cm core 0.2-0.3 cm edge	0.2-0.3 cm
Spatial range	≈ 30 cm	50-100 cm	≈ 50 cm
Rep. rate	10 Hz	100 Hz	5 Hz
Plasma duration	2-5 s	1000 s to CW	1000 s to CW
Port dimensions	7.5 cm diam.	1 x 2 m	10-50 cm diam?
Bakeout temperature	350° C		
Operating temperature	150° C		
Optics temp.			
Laser requirements			
Laser wavelength	~ 532 nm	~ 532 nm	~ 532 nm
Laser energy	0.5 J	5-10 J	?
Pulse length	30-40 ps	30-40 ps	10 ps
Chirp width	$\ll 1.5$ nm	$\ll 30$ nm	$\ll 1.5$ nm
Prepulse suppression	10^{-8} @ 532 nm 10^{-5} @ 1064 nm	10^{-6} @ 532 nm 10^{-4} @ 1064 nm	10^{-8} @ 532 nm 10^{-5} @ 1064 nm

The DIII-D plasma core is well diagnosed by a multi-laser conventional Thomson scattering system along a vertical chord. The divertor region has been shown to have profound effects on plasma confinement, however, the electron temperature and density

are measured only at the strike point and near the x-point. It is desirable to measure the electron temperature and density over this ~30 cm distance with a resolution of 0.2-1.0 cm. The available V1 port of 3" diameter requires a new LIDAR TS design, very different from the JET system, and along with cost constraints will limit the laser energy to ~0.4 J and the viewing system to between ~f/2.3 at the strike point and f/9 at the x-point. Spatial resolution for quantum statistical signal/noise ratio of 10 will be limited to ~1 cm, hence the laser duration should be 30-40 ps. The density is predicted by the UEDGE code to be in the range of $10^{19} - 10^{21} \text{ m}^{-3}$, with electron temperatures in the range of 0.5 - 50 eV. A repetition rate of the order of 10 Hz is desired. A higher repetition rate is desirable, but minimizing costs is more important.

We evaluate LIDAR Thomson scattering through a 3" top port V1 on DIII-D, although Figs. 4,5 show a bottom port. Despite the diameter of V1 being much smaller in diameter than side ports, it is enough closer to the divertor region, so that larger solid angle lenses are possible there than in side ports. Furthermore, no side windows can provide a view along the divertor between the strike point and the x-point without reflecting off the inner wall, which will be carbon (or carbonized) and will have a low reflectivity. Even from V1, a pair of mirrors are needed on both the laser and the viewing system to displace the view line about 22 cm from V1. Scattered light from the final laser mirror is evaluated in Section 2.4.2.

A lens train to transport light through the long - small diameter port, V1, would involve many small lenses, so we evaluated a fiber-optic system. We initially tried copying the JET LIDAR configuration with a central window for the laser, surrounded by 6 similar size windows for the viewing system. We soon found that this did not make effective use of the solid angle of the windows because the fiber optic cross-section was too small, as estimated below, to view the entire laser cross section. We also discovered that it was preferable to displace the viewing windows only in the toroidal direction from the laser window, because radial displacements would view the divertor channel tiles, greatly increasing the stray light. Chromatic dispersion in gradient index fiber optics was discussed in Section 2.5.

The total fiber optic cross section is determined as follows. The fiber optic cables from each lens must pack together at the spectrometer input, with a width determined by the wavelength resolution required ($20-40 \text{ \AA}$) divided by the linear dispersion of the spectrometer (34 \AA/mm for a particular f/1.8 instrument with a 2400 l/mm transmission grating). The numerical aperture of the graded index fibers is 0.20 which corresponds to a lens of f/2.5. By lens coupling to match the fiber optic numerical aperture exactly to that of the spectrometer, we gain an extra factor of 1.39 on the width of the input fiber bundle. Then the width of the fiber bundle is $(20\text{\AA})(1\text{mm}/34\text{\AA})(1.39)=0.82 \text{ mm}$

The height of the total fiber optic bundles is determined by the streak camera acceptance. LLNL cameras use streak tubes in which the photo-cathode extraction grid is made of parallel wires separated by 5 mm, rather than of a rectangular mesh, Fig. 9. The wires provide cylindrical electrostatic lens focusing of a photocathode image as high as 1.2 mm while still providing 10 ps time resolution, Fig. 8. The photo-cathode can accept photons from angles out to about 30° from normal corresponding to an f/0.87 input lens. We lens couple the spectrometer output to the streak camera with such a lens. The height of the f/2.2 bundle is then $(1.2 \text{ mm})(2.5/0.87) = 3.45 \text{ mm}$. The total area of the fiber bundle is 2.82 mm^2 .

To match the fiber optic bundles to the viewing lenses, we require that the fiber optic subtend the same solid angle from the optical center of the lens, that the lens subtends from the plasma. To ensure that every scattered photon reaching a lens from the plasma will also reach a fiber optic bundle, we evaluate the lens solid angle from the divertor strike point, the nearest plasma to the lens at a distance of about 30 cm, Fig. 10. The area of an individual bundle is the total fiber area.

divided by the number of lenses. We compute the number of lenses in linear arrays on either side of the laser injection tube. At the periphery of the 7.9 cm diameter tube, we allow 0.3 cm for structure and tolerances of the assembly that must slide into the V1 port on DIII-D. We allow 0.2 cm between lenses for structural material.

The optimum is 20 lenses of 0.86 cm diameter. This leaves most of the area of the 3" tube open and has a solid angle of 9.2×10^{-3} relative to 4π steradians, corresponding to a single lens of $f/2.6$ from the strike point, 10 cm away, or $f/10$ from the x-point, 40 cm away. Intensified streak cameras with a CCD camera readout are capable of detecting single photo-electrons. The quantum statistical signal/noise then depends on the number of photo electrons in the detector which is given by

$$N_{\text{Photo-electrons}} = N_{\text{photons}} r_0^2 n_e L \Omega T \epsilon_{QE} \epsilon_{\text{laser/view}}$$

The density required to yield 100 photo-electrons ($S/N=10$) is listed in Table 3 below. The terms in the equation are defined in the first two columns and in the following paragraphs. We assume a 0.4 J, 40 ps laser pulse of 2.1 cm diameter, and a viewing system/spectrometer/detector of 4.0 nm resolution.

Table 3. Minimum electron density for a quantum statistical signal/noise = 10.

<u>Factor</u>	<u>Symbol</u>	<u>Grating spectrometer</u>	<u>Prism spectrometer</u>
Photoelectron signal	$N_{\text{Photo-electrons}}$	100	100
Photons from laser	N_{Photons}	1.1×10^{18}	1.1×10^{18}
Thomson cross section (cm^2)	r_0^2	7.95×10^{-26}	7.95×10^{-26}
Electron density (cm^{-3})	n_e	$0.5-1.7 \times 10^{13}$	$1.1-3.7 \times 10^{13}$
Spatial resolution (cm)	L	1	1
Solid angle of viewing system from plasma	Ω	9.2×10^{-3}	1.9×10^{-3}
Viewing system transmission	T	0.113	0.26
Photo-cathode quantum eff.	ϵ_{QE}	0.21	0.21
Overlap of laser/viewing	$\epsilon_{\text{laser/view}}$	0.3-1.0	0.3-1.0

The viewing system transmission is the product of the component transmissions. These components and transmissions are listed in Table 4. Five lenses are used. One focuses the scattered laser light onto a fiber optic cable, a cylindrical lens is used to produce an elliptical view that provides a wide angle view of the laser beam from near the strike point to the x-point but excludes the divertor side tiles from view. A lens is used either side of the grating, and a second cylindrical lens is used before the streak camera to compress the image height to 1.2 mm. The fiber optic plate is used to remove the time dispersion caused by the grating, and is discussed in Section 2.5. The listed packing efficiency of the fiber optics is for graded index fibers. Minimizing the fiber length, together with the 1 cm spatial resolution, corresponding to 30 ps time resolution might allow standard fibers to be used.

Table 4. Viewing system light transmission.

Component	Number	Transmission
Mirrors near 45°	2	0.993 ² (OK ±40 nm)
Lenses:	5 (with 10 surfaces)	0.995 ¹⁰
Windows	2	0.995 ⁴
Fiber optic transmission	1 ~25 m	0.8
Fiber optic packing eff.		0.35
Grating transmission*	1	0.8
Fiber plate packing eff.*	1	0.55
Net transmission		0.113

* Not needed with prism spectrometer, use 0.995² for product of these two rows.

Mechanical tolerances and the precision required for machining and assembly become an issue with so many small parts. The optical path from a single fiber bundle to the intersection with the plasma and laser is shown in Fig. 6. We see that for perfect alignment, the viewing beam overlaps the laser beam for its entire length, in fact even at the strike point the viewed region of 4.75 cm diameter is considerably larger than the laser beam of 2 cm diameter. The tolerance on the 0.30 mm diameter fiber optic location is then $(0.30\text{mm})(4.75-2.0/4.75)/2 = \pm 0.0677 \text{ mm} = \pm 0.0027''$. This is within conventional machining tolerances.

Lenses approximating our optimum parameters of 8.6 mm diameter and 18.9 cm focal length are available. For example, Melles Griot has a precision laser grade achromat of 10 mm diameter and 20 mm focal length, with a tolerance of 1% on the focal length and a clear aperture of 90% of the diameter (9.0 mm) which yields an $f/2.22$, very near the desired $f/2.2$. In 12/90, each lens, product number 01 LAL 003 cost \$93.30 for a total cost of 4 k\$. The $\pm 1\%$ tolerance on focal length corresponds to $\pm 0.15 \text{ mm} = \pm 0.006''$, and results in a variation in image size of 0.047 mm or 20% of the fiber bundle diameter.

3.2. TPX

The TPX core Thomson scattering could be similar to the JET system,³ since large access ports are available. For an initial conceptual design, we assume the same viewing system optics. We switch from 5 J Ruby at 694.3 nm to a 1060 nm frequency doubled to 532 nm, which improves the photo-cathode quantum efficiency by factors of 4-8, and we modify the edge filter spectrometer to use a streak camera rather than photomultiplier tubes as a detector. We find that a 5-10 J laser is needed for 1 cm resolution, for the same signal/noise that JET achieves with 10-12 cm resolution. A minimum temperature requirement of 0.2 keV relaxes the chirp width requirements of the laser, and reduces the prepulse suppression requirement of the laser by allowing the use of laser line filters with a width of 10 nm and an attenuation of 10⁶.

A primary constraint on the TPX Thomson scattering system was the budget of 2510 k\$ in as spent dollars. If a LIDAR system can fit within that constraint, then the superiority of diagnosing a profile along a major radius, rather than along a fixed vertical line, coupled with the other advantages of LIDAR will be strong selling points.

TPX can use a system design at the midplane similar to that of JET, Fig. 1, as discussed earlier, but requires an order of magnitude higher spatial resolution. The higher spatial resolution at

present requires a streak camera detector for the 8-40 ps response time needed to resolve 0.2-1.0 cm, thinned micro-channel-plate (mcp) photomultiplier tubes can achieve 40 ps response,⁷ so could be used in the 1-2 cm resolution range. By year 2000, faster detectors may be available, but will probably be limited by aperture effects: an aperture can close or open no faster than the ~30 ps/cm that a voltage pulse can propagate.

In order to use an edge filter spectrometer with a streak camera, the filter outputs must be arranged so that they can all be projected onto the input of the streak camera with path lengths nearly equal. Such a system is shown in Fig. 11, where successive filters are rotated to reflect each wavelength range radially at a different angle. Mirrors near 45°, with radial distances adjusted to equalize path lengths, reflect each wavelength towards a lens which focuses the light into a linear array on the streak camera input. Exact path length equality is unnecessary, since the streak camera time base output can be individually calibrated for each channel.

The use of a 1060 μm laser, frequency doubled to 532 nm, rather than the 694.3 nm ruby laser used in JET, significantly increases the quantum efficiency of the streak camera photo-cathode. An S-20 cathode is a factor of 4.6 times more efficient at 532 nm, and an 111 photo-cathode, provides a factor of 7.5 higher efficiency over the JET system.⁶ This change alone provides most the extra sensitivity needed to achieve a spatial resolution of 1 cm. Doubling the laser power from 5 J to 10 J will provide the same signal/noise ratio with 1 cm spatial resolution that JET achieves with 12 cm resolution.

Further study of the viewing system is required to determine whether the goal 0.2-0.3 cm resolution is achievable near the plasma boundary. If so, then the laser duration should be near 10 ps, rather than 30-40 ps. The boundary is somewhat closer to the windows, so the larger solid angle will help. The boundary electron temperature is also lower, resulting in a narrower Thomson scattered spectrum, which can be more easily detected, but which requires closer spacing of spectrometer channels near the laser wavelength that may not be compatible with a filter spectrometer, and which is less compatible with using a laser notch filter to reduce stray laser light by 10⁶ over a 10 nm width. Additional alternatives to the JET design should be evaluated for improved performance or reduced cost.

3.3. ITER

We evaluated LIDAR Thomson scattering for application to the ITER core, edge, and divertor. The core and edge system is shown in Fig. 12. Our designs differ from other ITER designs in using a chirped pulse amplification laser² of ~10 ps duration; a prism spectrometer which maintains a constant optical path length over its entire aperture, as required for high-spatial-resolution LIDAR (A filter spectrometer, Fig. 11, is satisfactory for the core); and a streak camera detector followed by a CCD camera for either location, with photomultiplier tubes and digital recorders an option for the core system.

We find that a 100 Hz, 10 ps, 0.6 J laser would provide core resolution of 5 cm down to a density of 10¹⁸ m⁻³, edge resolution of 2 mm down to 2 × 10¹⁹ m⁻³, and divertor resolution of 2 mm down to 10²⁰ m⁻³. Higher energy, or reduced resolution are necessary to extend to lower densities. Each limit is for 600 detected photons, giving n_e and T_e to 10%. The core and edge systems could be combined, using a beamsplitter with 2 streak cameras. An opportunity exists for a significantly improved divertor line-of-sight, by amending the system requirements to align the intercoil structure vanes with the SOL.

Prism dispersion is lower than that of a grating, but is adequate with lens coupling of the spectrometer to the streak camera with magnification, particularly if cylindrical lenses are used to focus more of the light into the slit area.

Core and edge systems could be combined, with beamsplitting to 2-streak cameras. The core system resolution requirement of 5 cm allows the use of photomultiplier tubes and digital recorders with ~150 ps time response. The systems could share a neutron maze, periscope system similar to that proposed for the core, by Salzmann, et al.³ For the core, slowing the streak camera sweep speed would yield a pixel limited spatial resolution of about 5 cm across the entire core. A faster edge streak camera could yield 2 mm resolution over the outer 24 cm regions. The edge location can be adjusted by varying the timing of the streak camera trigger. The core sensitivity is higher, so most of the light could be sent to the edge camera. A single streak camera can also change streak speed during the streak¹⁰ to perform both edge and center, but the total of ~120 pixels must then be apportioned between the two regions. Edge design features are listed below:

- The minimum density is 10^{20} m^{-3} at 5 cm resolution, and $\sim 2 \times 10^{19} \text{ m}^{-3}$ at 2 mm resolution with a 0.3 J, blue laser, f/4.5 final mirror, and viewing system transmission of 0.3. Both n_e and T_e are determined to 10% with approximately 100 counts in each of 6 spectral channels. Lower densities could be measured either by slowing the streak camera for poorer spatial resolution or using a higher power laser.
- The laser is focused near the plasma edge to allow the laser beam to expand to a larger diameter and deliver a lower power density, below the wall ablation limit, on the inner wall. This also allows a smaller access hole in the neutron shield reducing neutron leakage if it isn't shared with the core system. If the focus point is just outside the plasma edge, power densities exceeding could provide a spatial fiducial.
- The distance from the final focusing mirror to the focus is ~3 m, providing an 18 ns time difference between laser light backscattered from the final optic and the Thomson scattered signal from the plasma, sufficient time to gate the streak camera photocathode, deflection plates, and/or mcp intensifier to reduce scattered laser light from the final optics by 8 orders of magnitude to the order of the signal. This allows the viewing system to share optics with the laser. It has the advantage of true 180° backscatter, rather than near 180° as on JET, providing complete overlap of the viewed region with the laser illuminated region.

In the divertor we propose to measure along the SOL from the strike point towards the X-point, rather than measuring across the width of the SOL which has a high probability of missing the most interesting region. This is the optimum line-of-sight, since the location of a gas target divertor ionization front along the SOL is unknown.¹¹ Some features and issues are:

- Intercoil structure vanes fill the region between toroidal field coils below the strike point.¹² By requiring that the vanes be aligned with the SOL above the strike point, a neutron maze similar to that proposed by Salzmann, et al.,³ can be used. The maze can be arranged with the optical path between vertical field coils.
- The hole diameter in strike plate needs to be large for a large signal and a long, non-vignetted view path, but needs to be small for minimum degradation of strike plate cooling. A compromise might be to use a small hole to pass the laser beam, surrounded by other small holes to view the beam. For an f/10 mirror, 3 m away, the holes would fill a 30 cm circle, and provide non-vignetted data to beyond the X-point. Care will be necessary to avoid blind spots.

- Laser power densities exceeding $\sim 10^{14}$ W/cm² near the focus will ionize gas; the resulting plasma density will be comparable to the divertor plasma for pressures near 10^{-2} Torr. This region could extend 0.6 cm either side of the focus with a 3 J laser. By locating the focus at least 2 cm below the strike point, the focus-plasma will provide a spatial fiducial, with a zero density region between the fiducial and the strike point to avoid perturbing the data.

Focusing a short pulse laser system within the plasma may be unsuitable for Thomson scattering because above some power density limit, non-linear effects will perturb the plasma electron density and axial velocity, as discussed in the next section.

4. Physics issue and design of experimental test

We designed an experiment to demonstrate LIDAR Thomson Scattering with a spatial resolution of a few millimeters in a low density ($< 10^{17}$ cm⁻³), incoherent scattering regime plasma, appropriate to magnetic fusion type parameters, Fig. 13. The principle physics issue is to determine the power density limit for Thomson scattering, above which it cannot measure electron temperatures because non-linear effects create a significant axial electron velocity exceeding the thermal velocity. (Near 180° LIDAR Thomson scattering measures the electron velocity component that is parallel to the laser propagation direction.) Non-linear mechanisms that change the axial electron velocity or density include the ponderomotive force^{13,14} acting along the axial gradient of power density of an $\sim f/3$ focusing mirror, and figure-8 electron orbits in the E×B field at high power densities. Linear mechanisms include the parallel component of the laser E-field in a finite f /number focused beam, or a laser polarization in the scattering plane rather than orthogonal to it.

We designed an experiment to test the nonlinear power density limits using the Janus laser facility¹⁵. A schematic layout of the target chamber is shown in Fig. 14 and of the spectrometer and detector in Fig. 15, and is described below:

The conventional limit requires the oscillation velocity, v_{osc} of an electron in the laser field to be less than the electron thermal velocity,¹⁶ resulting in a power density limit of 4×10^{15} W/cm² at 532 nm for $T_e = 100$ eV ($P/A \propto T_e \lambda^2$) as shown in Fig. 16. This limit is violated by orders of magnitude in recent laser gas-jet plasma experiments,^{17,18} implying that the conventional limit is incorrect. From standard theory¹³, we predict that power densities of 3×10^{17} W/cm² (which should be accessible in the Janus Facility¹⁵) will perturb both the density and axial electron velocity.^{11,12} The wrong laser polarization would become apparent near the 10^{15} W/cm² region.

1. A separate 0.1 - 1 ns heating laser will ionize the gas target, decoupling ionization from the probe laser intensity. A 1 μ m laser would be preferred since that would reduce detection by an S-20 LLNL streak-camera by several orders of magnitude. If this beam is polarized, it should be orthogonal to the plane of scattering.
2. A gas target: Initially a static fill of hydrogen or helium will provide a known density to calibrate the Thomson scattering sensitivity when ionized by sufficiently high power density from the heating laser, if the size of the plasma can be independently measured. Subsequently, most of the work will be done with a pulsed gas jet target. Densities in the 10^{15} - 10^{16} cm⁻³ range are preferred

(10^{17} cm^{-3} begins to be dominated by Raman scattering, $<10^{14} \text{ cm}^{-3}$ has too little signal). Depending on the range of power densities available from the laser, we may want to locate the gas jet away from the focus for some experiments. Argon, or other gases, might also be satisfactory, but we need to avoid additional ionization by the probe laser. The low plasma density keeps the experiment in the incoherent scattering regime, where the electron temperature and density are measured, but no information is obtained about ion temperatures.

3. A 1 ps probe laser with bandwidth $\leq 1 \text{ nm}$ (\ll Thomson scattering spectral width), frequency doubled to $0.4 \mu\text{m}$, and the $0.8 \mu\text{m}$ component removed, for high efficiency with the S-20 streak camera. Frequency doubling also reduces prepulse that can contribute to stray light. The counter-propagating geometry seems OK. Power densities exceeding $\sim 5 \times 10^{17} \text{ W/cm}^2$ are needed to demonstrate the limits to Thomson scattering validity for measuring thermal electron velocity distributions. Power densities well below 10^{15} W/cm^2 are needed to obtain $v_{osc} < v_{th}$ to satisfy the conventional criterion (Fig. 14 and Sheffield¹⁶, "Plasma Scattering of Electromagnetic Radiation", p. 20). We need to vary the timing of this pulse within and after the heating pulse.
4. Effective dumps for both lasers. Stray laser light from the heating or probe lasers will be the main difficulty.
5. A viewing system at near 170° to transmit backscatter from the probe laser to a spectrometer and detector. The viewing system looks through the laser focus/gas jet to a viewing dump, and will be lens or mirror coupled to a spectrometer/streak camera detector system.
6. An LLNL S-20 photocathode streak camera, with intensifier, and CCD camera and data acquisition computer will provide near 10 ps time response.
7. A Hilger prism spectrometer. A prism is necessary to keep all optical path lengths equal within the 1.5 mm spatial resolution that I want to achieve. To compensate for the low dispersion, I expect to lens couple the spectrometer to the streak camera with a magnified image. (Another possibility might be to build a stepped fiber optic plate to correct a grating spectrometer to give a nearly constant optical path. I could live with the reduced spectral resolution.)

We envision 2 scans would be needed:

- A. Vary the probe laser power density, to determine the limit for valid Thomson scattering measurements of thermal electrons. Possibly include a scan with the laser polarization in the scattering plane, which should yield a much lower limit. Then operating within these limits –
- B. Vary the size or profile of the plasma to demonstrate spatial resolution of near 1.5 mm. One method might be to change the size of the gas jet nozzles, another would be to insert a wake producing obstacle into the jet, still another would be to move the plasma by small increments, and show that the scattered signal shifted appropriately in time.

The difficulty of this experiment is largely determined by the Thomson scattering signal level (stray laser light is the other critical issue), which is given by

$$N_{\text{Photo-electrons}} = N_{\text{photons}} r_0^2 n_e L \Omega T \epsilon_{QE} \epsilon_{\text{laser/view}}$$

The density required to yield 1000 photo-electrons (S/N=10 in each of 10 equal channels) is listed in Table 5 below. The terms in the equation are defined in the first two columns. We assume a 0.5 J, 1 ps laser pulse to make a preliminary estimate of the minimum density usable with Thomson scattering on the Janus facility.

Table 5. Minimum electron density for a quantum statistical signal/noise = 10 in 5 equal channels.

<u>Factor</u>	<u>Symbol</u>	<u>Prism spectrometer</u>	
Photoelectron signal	$N_{\text{Photo-electrons}}$	1000	
Laser photons (0.5 J, 0.4 μm)	N_{Photons}	1.03×10^{18}	
Thomson cross section (cm^2)	r_0^2	7.95×10^{-26}	
Electron density (cm^{-3})	n_e	2×10^{14}	Minimum for S/N=10.
Spatial resolution (cm)	L	0.03	
Solid angle of viewing system from plasma	Ω	0.0314	For f/5
Viewing system transmission	T	0.25	
Photo-cathode quantum eff.	ϵ_{QE}	0.25	
Overlap of laser/viewing	$\epsilon_{\text{laser/view}}$	1.0	

Our conclusion is that the experiment looks feasible, if stray laser light can be sufficiently minimized, and that we could address some fundamental physics issues that have not been previously studied.

Acknowledgments

We acknowledge the support of Robert Schock, Keith Thomassen, and John Holzrichter in providing the LDRD funding for the work – Project 94-ERP-024. Brad Rice initiated this project. Joe Kilkenny, Peter Young, and Chris Darrow provided suggestions and encouragement, and the potential use of facilities. Hoang Nguyen provided patient education in short pulse laser technology. Allen Costley of the ITER Joint Central Team provided comments and drawings for our use.

*This work was performed under the auspices of the U.S. Department of Energy by Lawrence Livermore National Laboratory under contract No. W-7405-Eng-48.

References

1. H. Salzmann, J. Bundgaard, A. Gadd, et al., Rev. Sci. Instrum. **59**, 1451 (1988); and H. Salzmann, K. Hirsch, J. E. Gruber, et al., Rev. Sci. Instrum. **56**, 1030 (1985).
2. M. D. Perry and F. Mourou, "Terawatt to Petawatt Sub-ps Lasers,": Science **264**, 917 (1994).
3. H. Salzmann, et al., DRAFT Report: "Thomson Scattering in the Core, Edge and Divertor of ITER." Dec. 1994.

4. B. C. Stuart, M. D. Feit, A. M. Rubenchik, B. W. Shore, and M. D. Perry, *Phys. Rev. Lett.* **74**, 2248 (1995).
5. R. A. Lerche, et al., "Resolution limits and optimization of the LLNL streak camera focus," *Proc. of SPIE Hi-Speed Photography, Videography & Photonics V* **832**, 266 (1987).
6. Illes P. Csorba, "Image Tubes," Howard W. Sams & Co., Inc., Indianapolis, Indiana (1985) p. 209.
7. P. M. Bell, J. D. Kilkenny, O. L. Landen, et al., *Rev. Sci. Instrum.* **63**, 5072 (1992).
8. C. E. Thomas, Jr., E. A. Lazarus, R. R. Kindsfather, et al., *Rev. Sci. Instrum.* **57**, 1819 (1986).
9. B. W. Brown, C. W. Gowers, P. Nielsen, B. Schunke, *Rev. of Sci. Instrum.* **66**, 3077 (1995).
10. A. H. Lumpkin, *Nuclear Instr. and Methods in Physics Research Section A – Accelerators, Spectrometers, Detectors, and Associated Equipment* **304**, 31 (1991).
11. D. Post, et al., "ITER Divertor modeling:" IAEA-CN-60/E-P-7, Seville, (1994).
12. R. Bulmer, private communication, ITER Drawing 095039.
13. W. L. Kruer, "Phys. of Laser Plasma Interactions," (Addsn-Wsly, Redwood City, CA, 1988).
14. C. B. Darrow, et al., *Phys. Rev. Lett.* **69**, 442 (1992).
15. P. E. Young, J. H. Hammer, S.C. Wilks, and W. L. Kruer, *Physics of Plasmas* **2**, 2825 (1995).
16. John Sheffield, "Plasma Scattering of E-M Radiation," Academic Press, NY, 1975, p. 20.
17. T. E. Glover, et al., *Phys. Rev. Lett.* **73**, 78 (1994).
18. A. A. Offenberger, et al., *Phys. Rev. Lett.* **71**, 3983 (1993).

JET Main and Divertor LIDAR Thomson scattering system

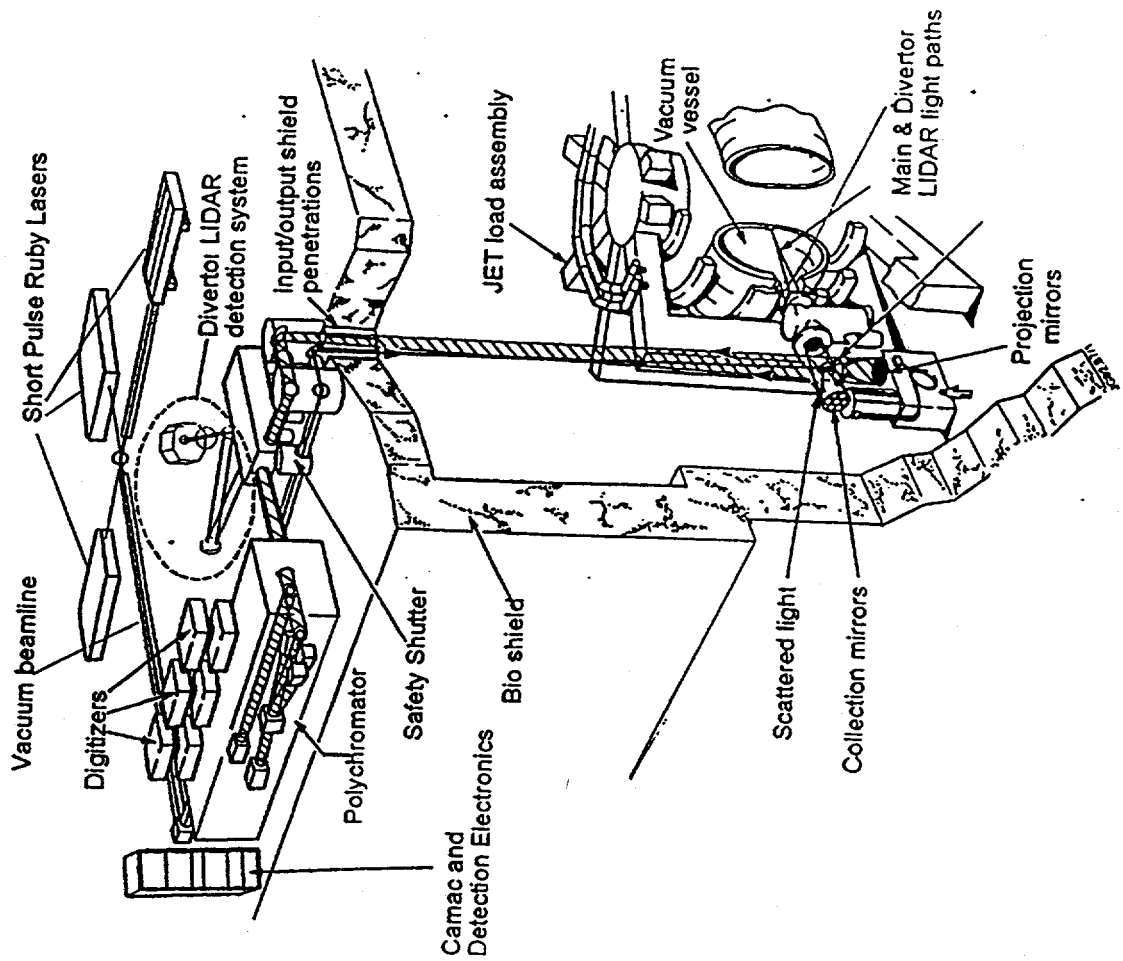


Fig. 1. Layout of the JET LIDAR Thomson scattering system.

Intense short pulses are produced by chirped-pulse amplification

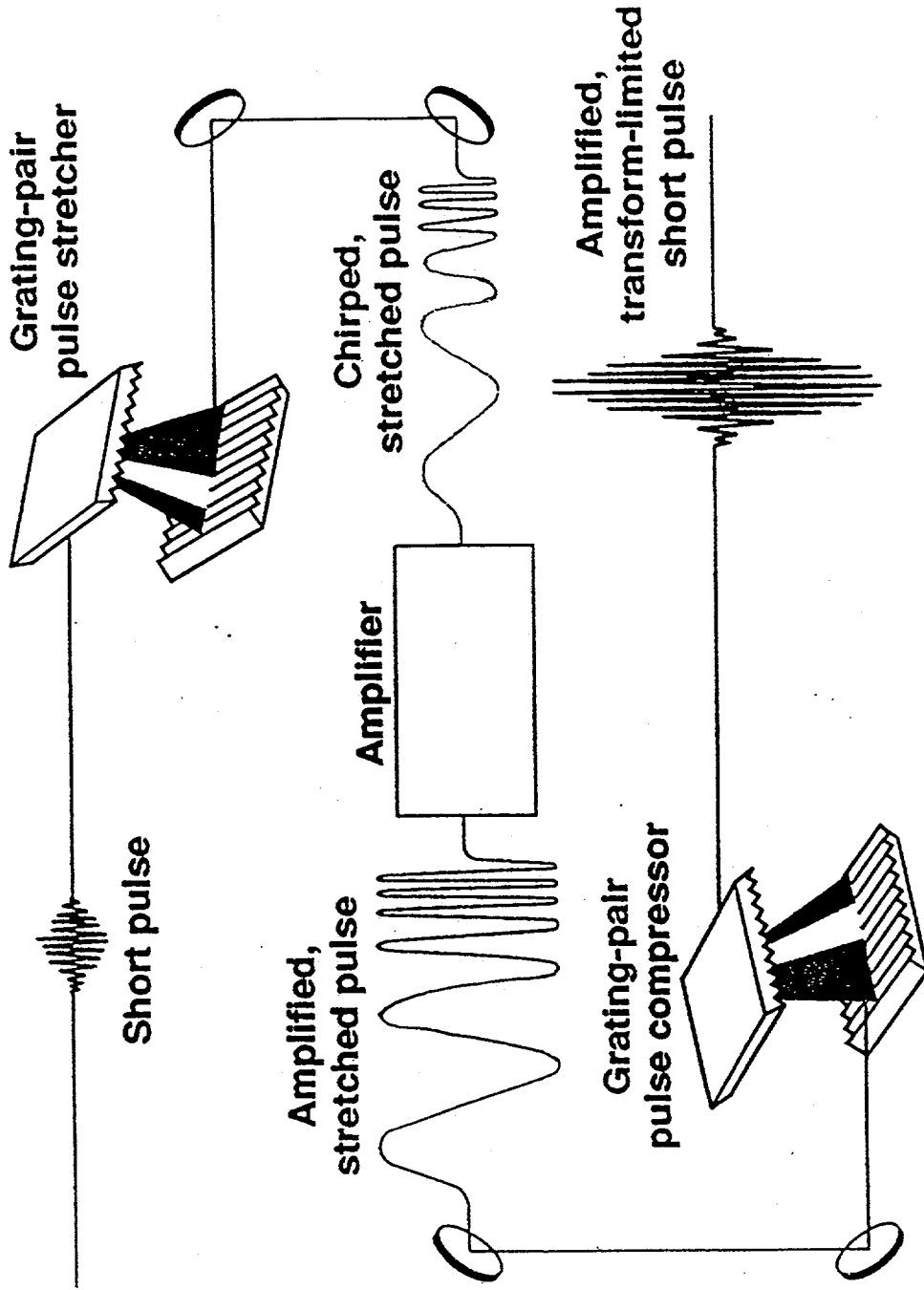


Fig. 2. Intense short pulses are produced by chirped-pulse amplification.

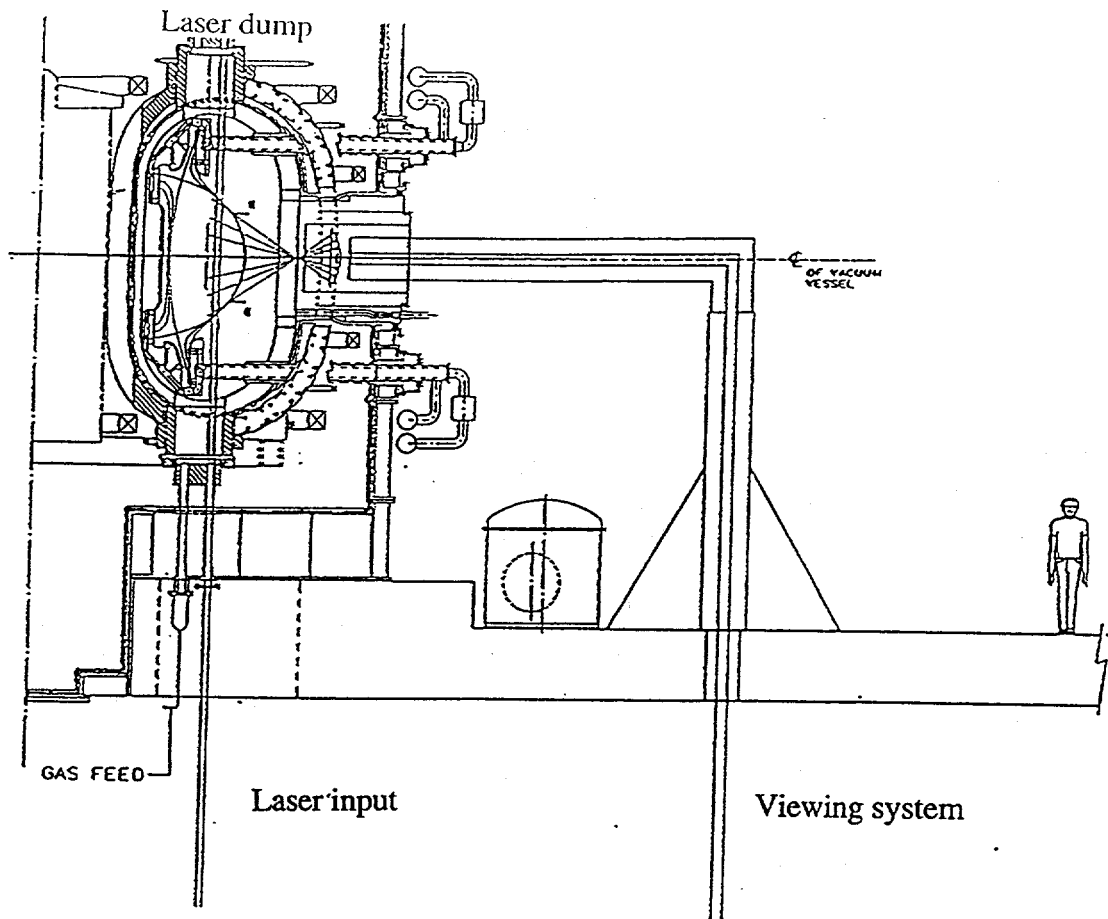


Fig. 3. TPX tokamak with a conventional Thomson scattering system.

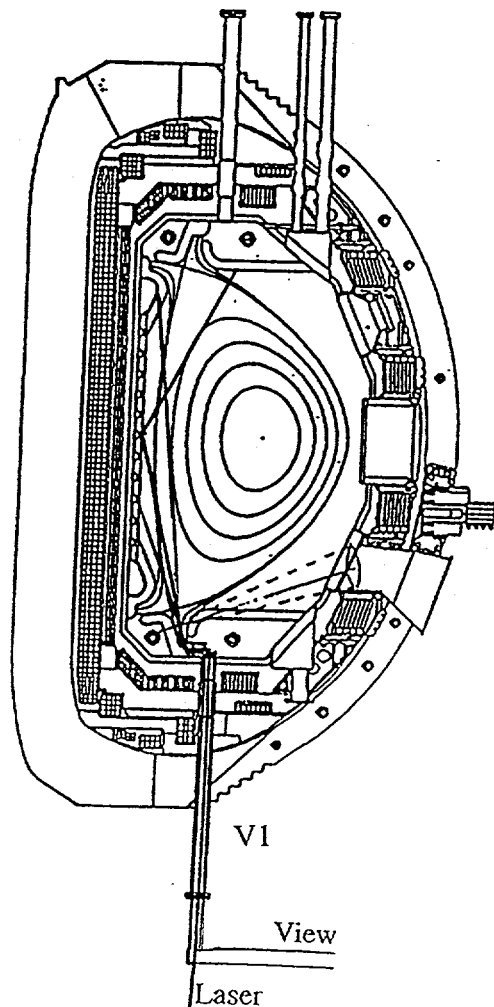


Fig. 4. DIII-D with LIDAR Thomson scattering in the divertor, where a conventional viewing system is blocked by divertor tiles.

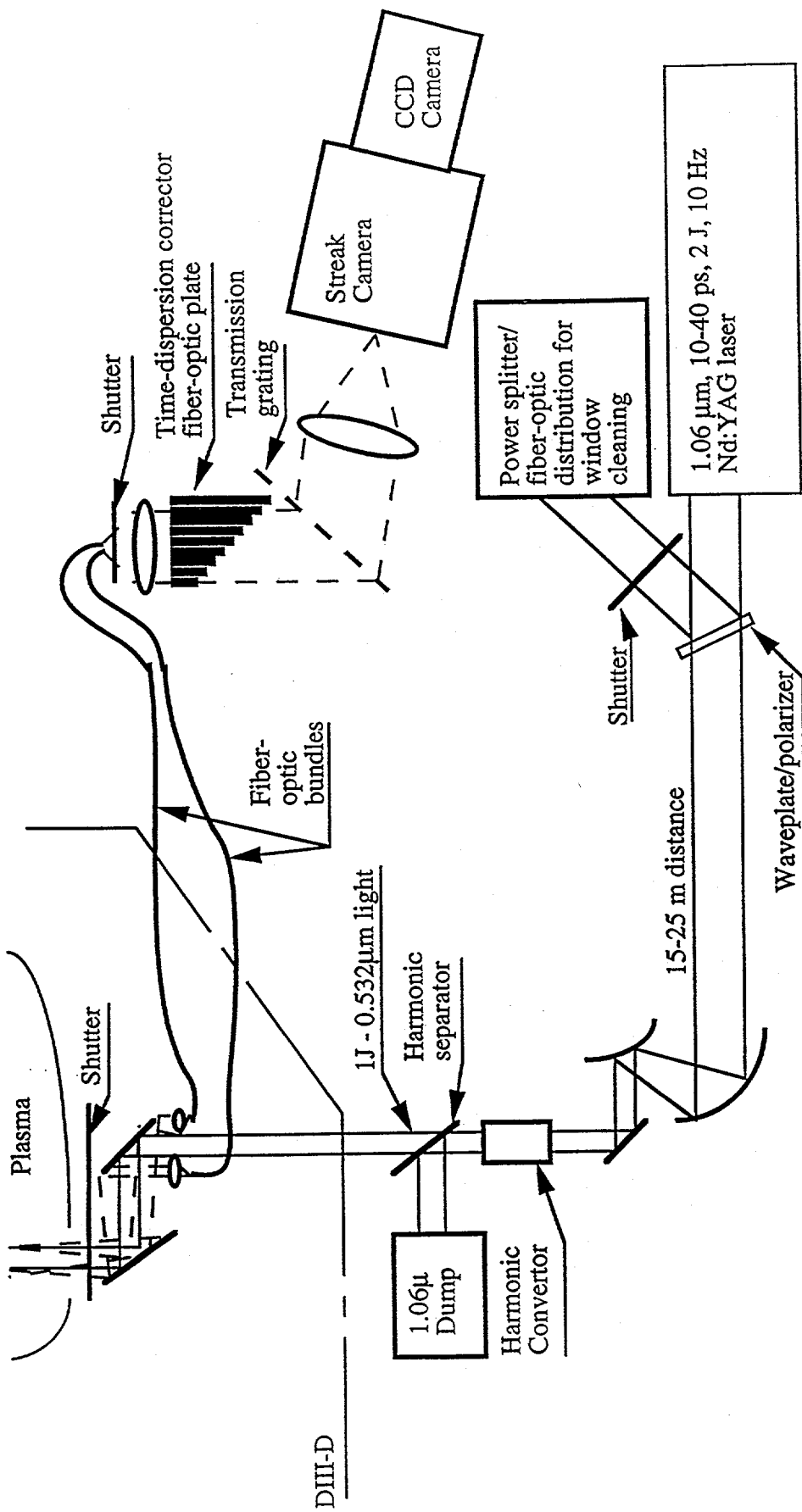
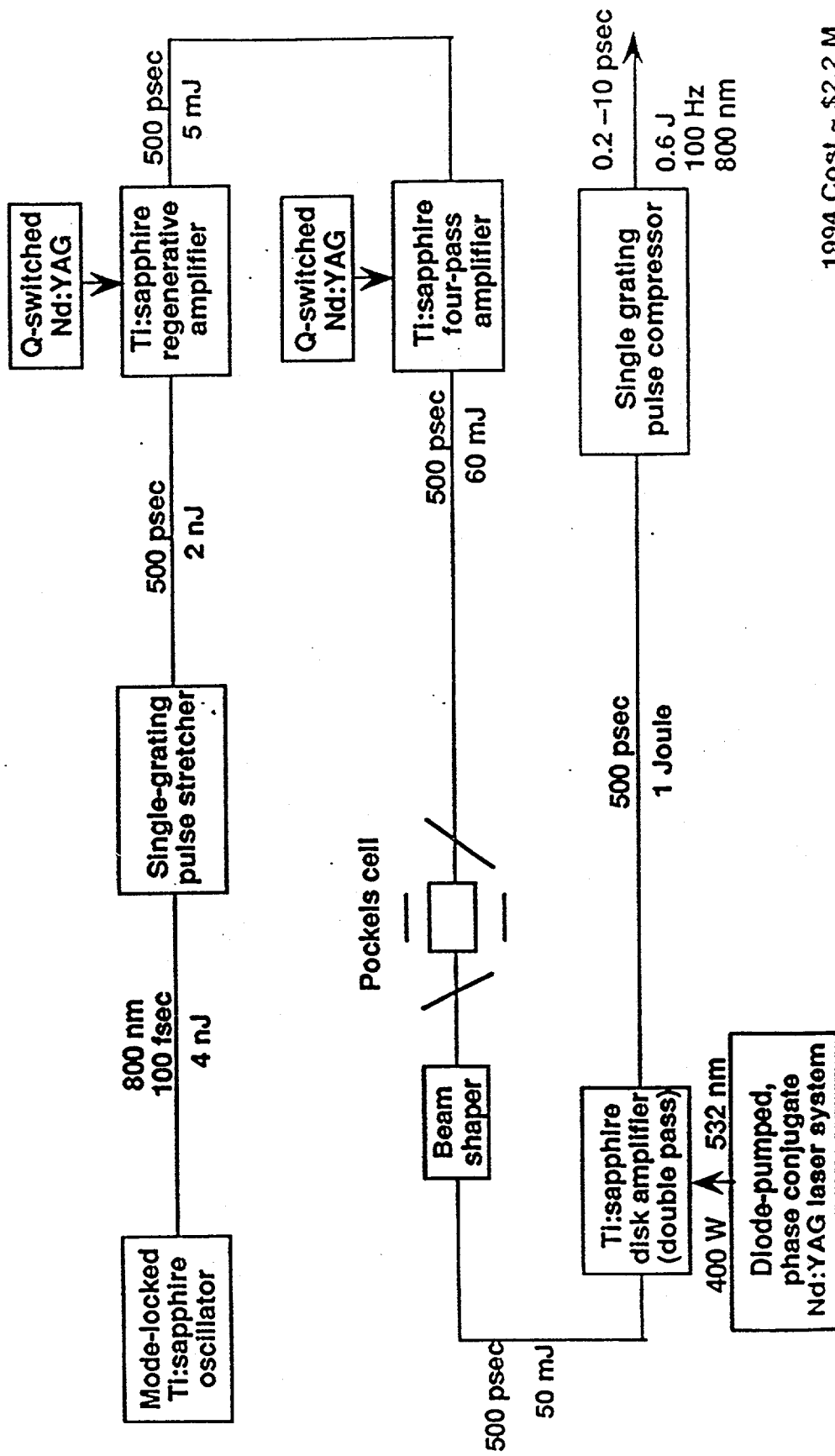


Fig. 5. Schematic of LIDAR Thomson scattering installed through a V1 port of DIII-D to diagnose a high triangularity divertor between the strike point and the x-point. Components are shown for correcting time dispersion, removing 1.06 μ m light, and performing ablative window cleaning.

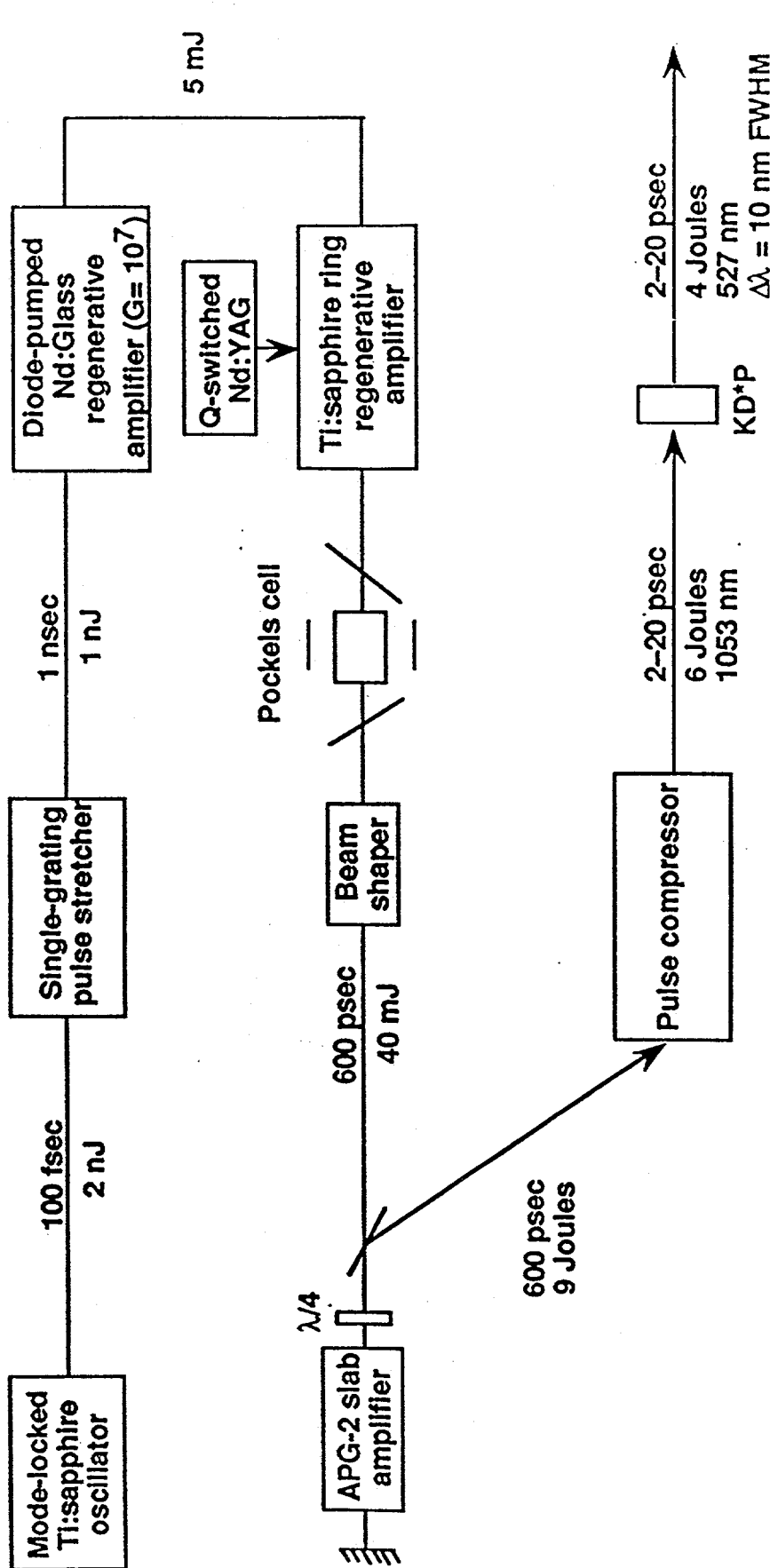
100 Hz operation at 800 nm can be achieved at reduced pulse energy (0.6J) and increased cost



1994 Cost ~ \$2.2 M

Fig. 6. 100 Hz operation at 800 nm can be achieved for 0.2-10 ps pulse durations at reduced pulse energy (0.6 J) with diode pumping for a cost of 2.2 M\$.

A hybrid CPA laser system utilizing a flashlamp-pumped APG-2 slab amplifier can produce 6 Joules, 2-20 psec pulses at a 3-5 Hz repetition rate



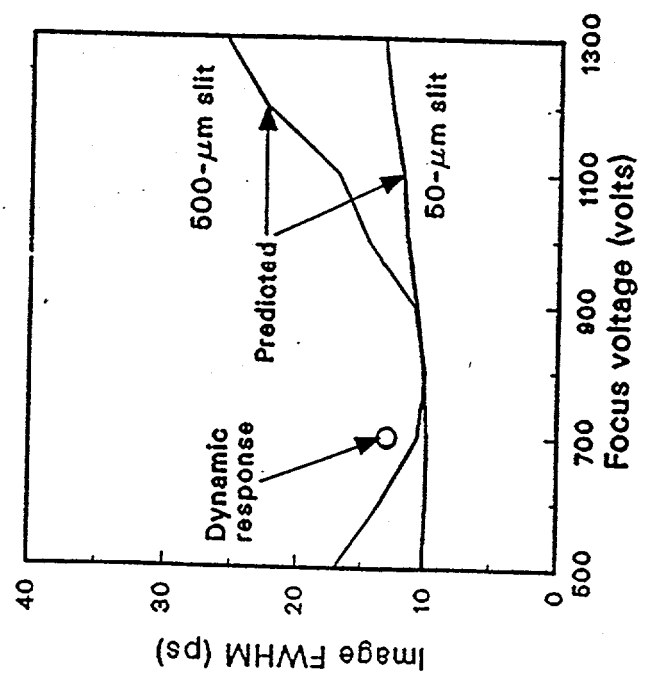
1994 Cost ~ \$1.5 M

Fig. 7. 3-5 Hz operation at 527 nm can be achieved for 2-20 ps pulse durations at 6 J with flashlamp pumping for a cost of 1.5 M\$.

Streak camera time response



- Measurements show a time response (full-width-half-maximum) of ≈ 10 ps for the ITT F4157 streak tube



The dynamic response was made using a 1-ps, 0.605 μm dye laser passed through an etalon to produce a set of pulses spaced 296 ps apart

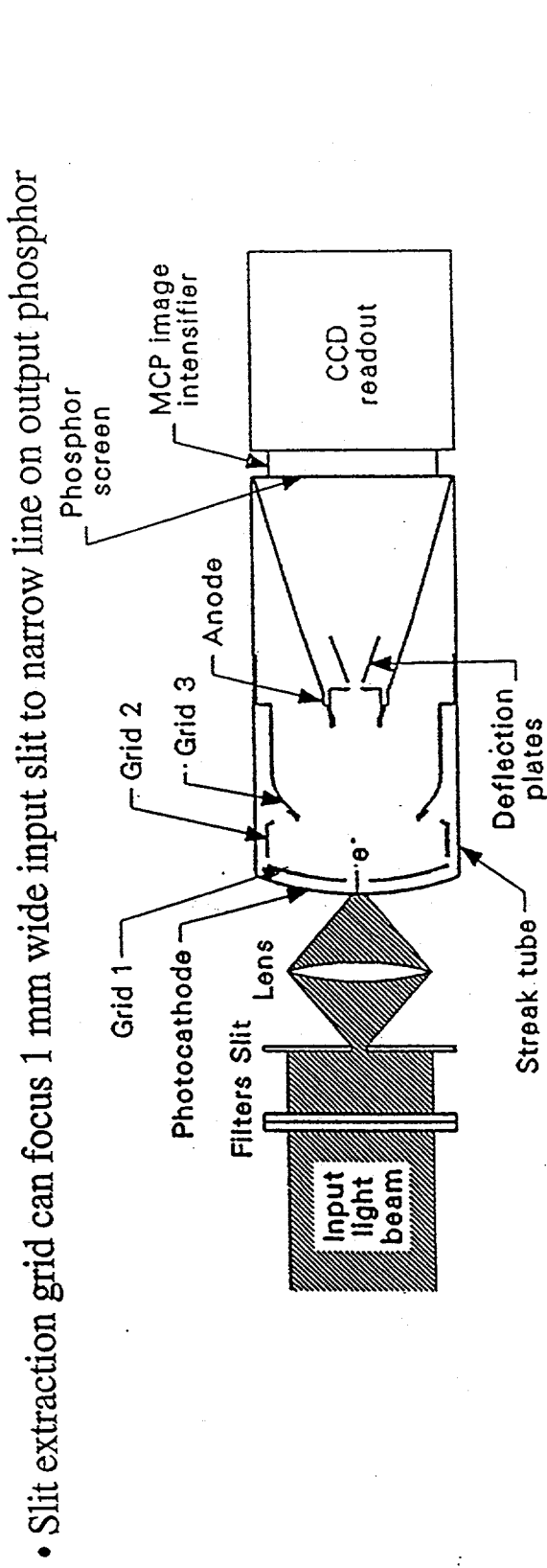
The "predicted response" was calculated from the measured image width, Δx and sweep speed, S and an axial energy spread $= 0.5$ eV of the photoelectrons

The response is in good agreement with calculated electron trajectories

Ref.: R.A. Lerche, et al., UCID-21258 (Nov 1987).

Fig. 8. Streak camera time response of ~ 10 ps is achieved, even with a 500 μm wide slit.

Streak cameras feature 100-200 time resolution units, single photo-electron detection on CCD, and wide dynamic range



- One photoelectron yields ~100 photons from phosphor, detectable by intensified CCD camera
- Dynamic range of mcp intensifier is ~80/pixel, binning 4 pixels (out of 576) in time and 50 pixels (out of 384) in wavelength yields up to 16,000 photoelectrons per resolution element.
- Increased dynamic range may result from Phillips/Thomson developing CCD detector build into streak camera, eliminating mcp and phosphors.

Refs: 1. R. A. Lerche, E. L. Grasz, R. L. Griffith, R. A. Simpson, R. Posey, "Resolution limitations and optimization of the ITT F4157 streak tube focus for fast (10 ps) operation" LLNL Report UCID-21258, Nov. 1987.
2. R. A. Lerch, D. S. Montgomery, J.D. Wiedwald, "High-contrast ratio power measurements with a streak camera", LLNL Report UCRL-JC-106484, 1991.

Fig. 9. Schematic of LLNL streak camera with ITT F4157 streak tube.

Viewed volume in divertor intersects laser from strike point to beyond x-point in DIII-D

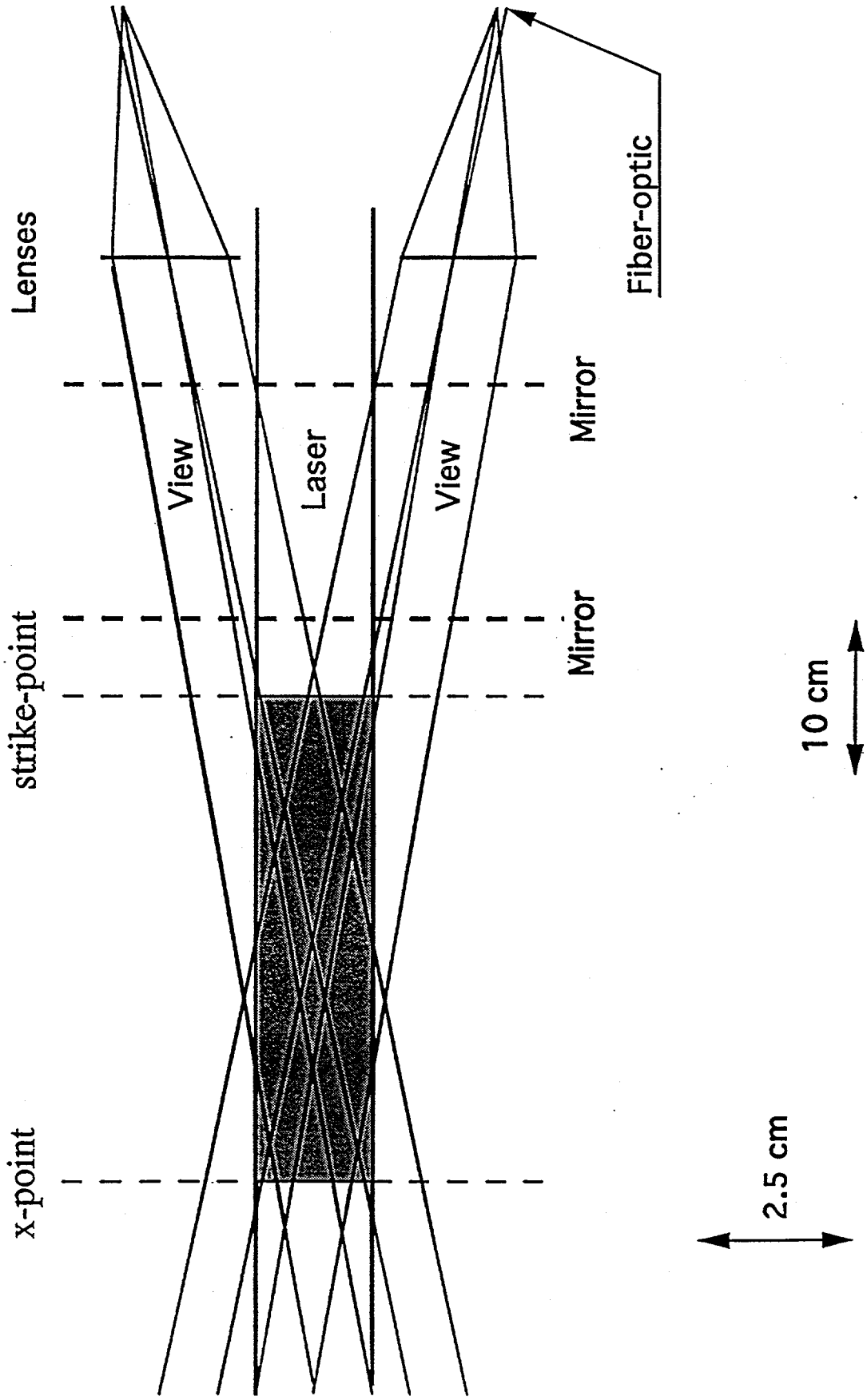


Fig. 10. Overlap of viewed and laser filled volume, and focusing into fiber optic

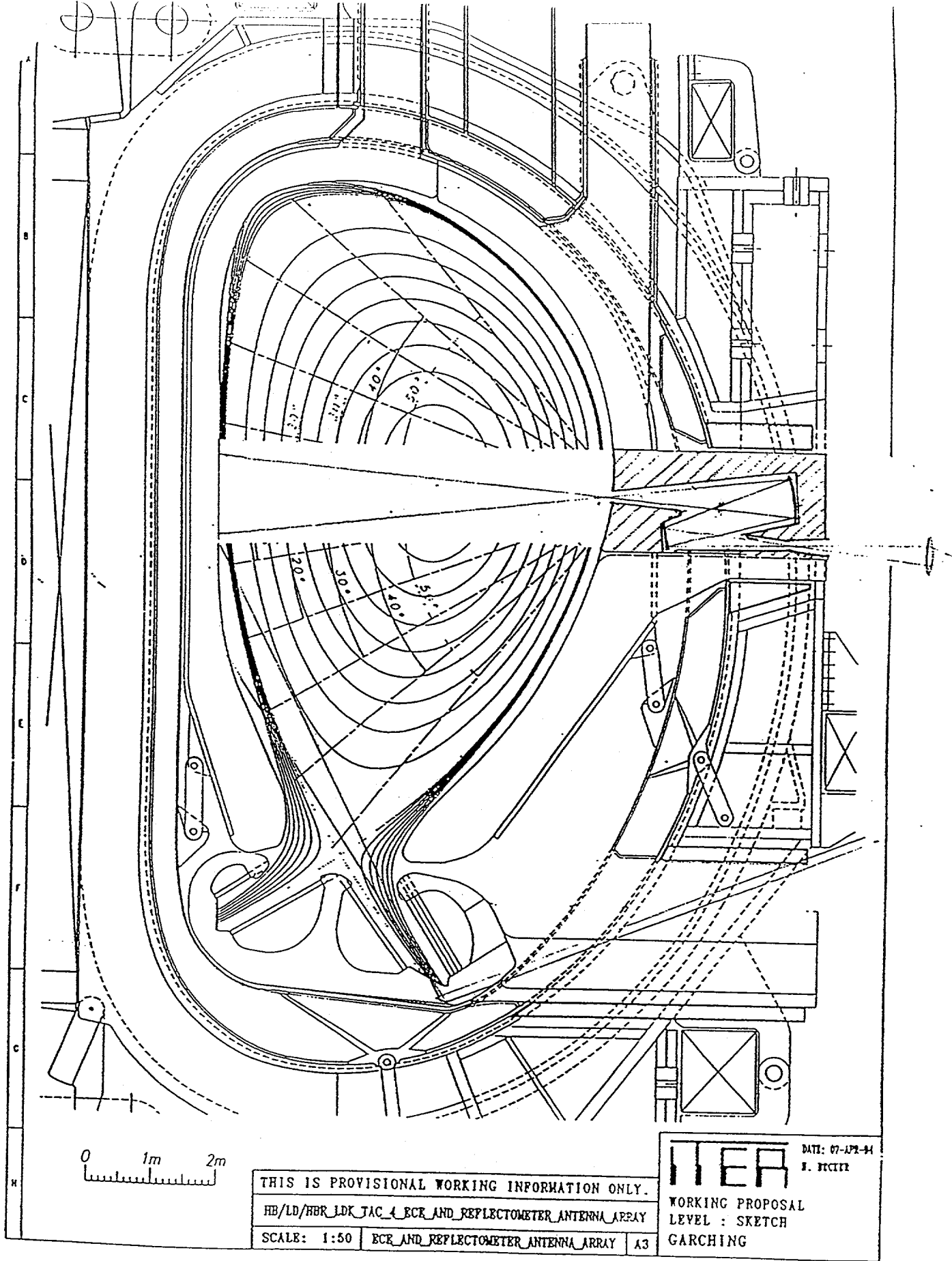


Fig. 12. Drawing of ITER minor cross section with LIDAR neutron-shielded periscope sketched in.

LIDAR Thomson Scattering Experiment to demonstrate millimeter resolution

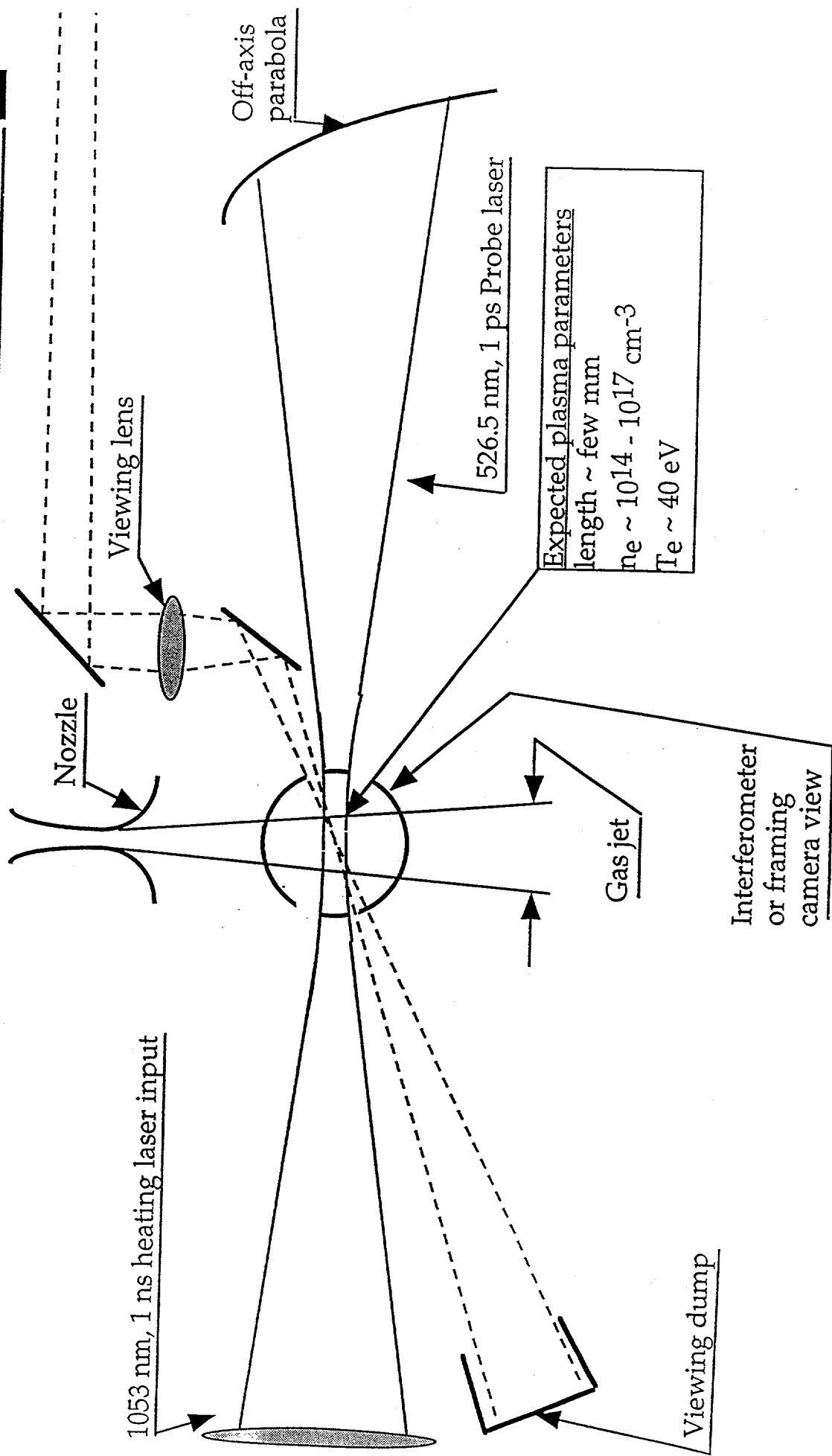


Fig. 13. LIDAR Thomson scattering experiment to demonstrate millimeter resolution and test nonlinear power density limit for Thomson scattering.

Scale 10"/1"

Horizontal Dispersion
R-Plot 575511

Not to scale

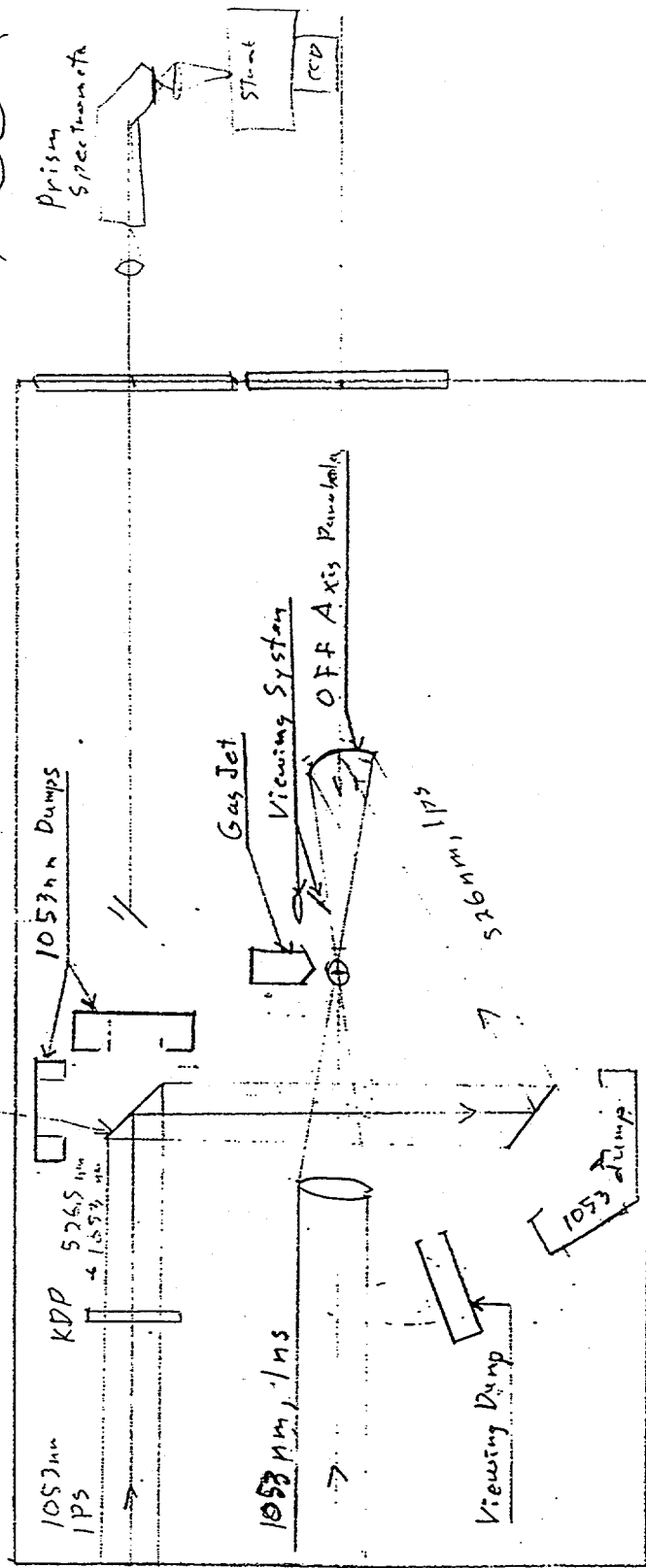


Fig. 14. Plan view of Janus laser target chamber, with added components for LIDAR Thomson scattering experiment.

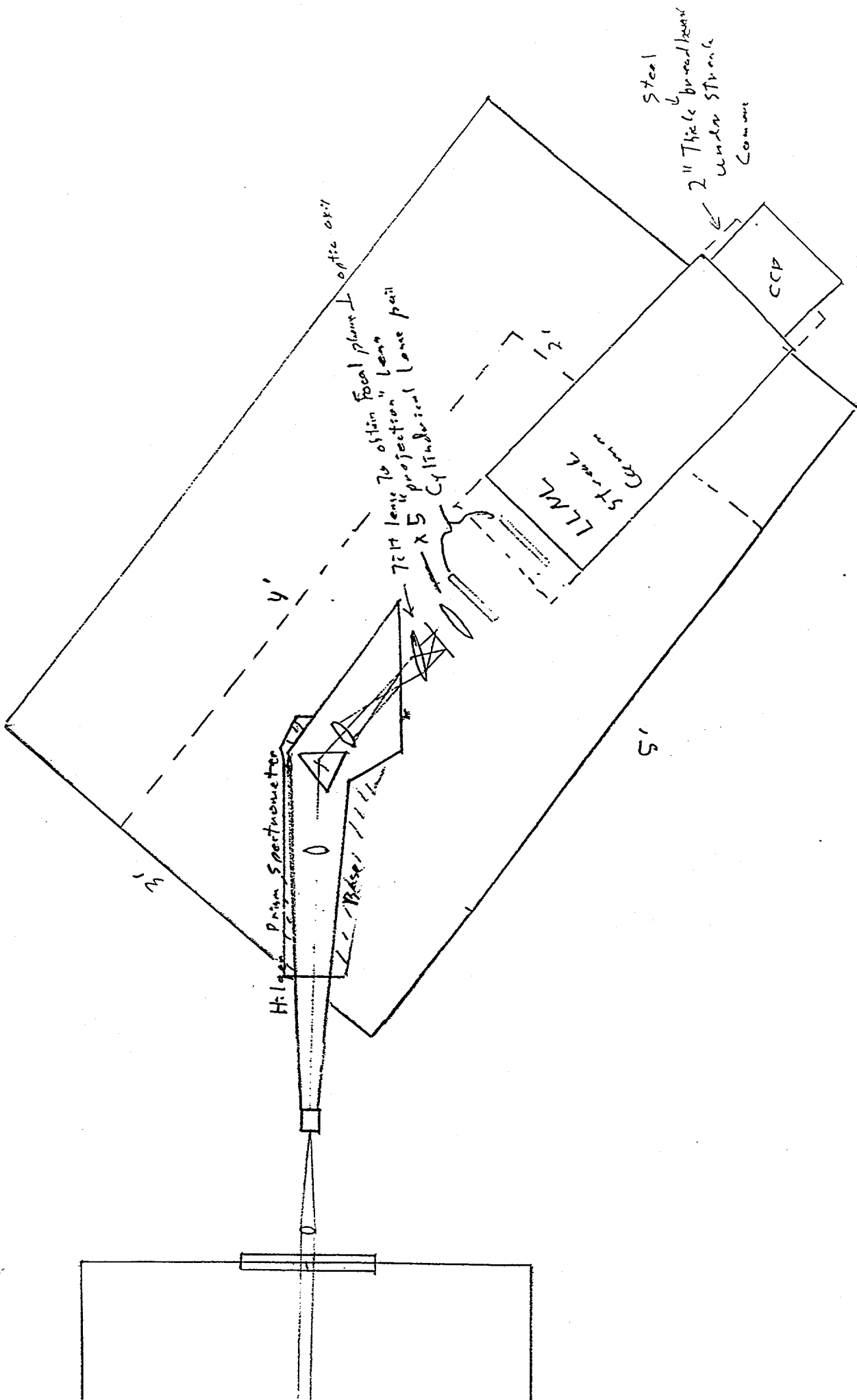


Fig. 15. Plan view of prism spectrometer, streak camera, and CCD camera with lens coupling.

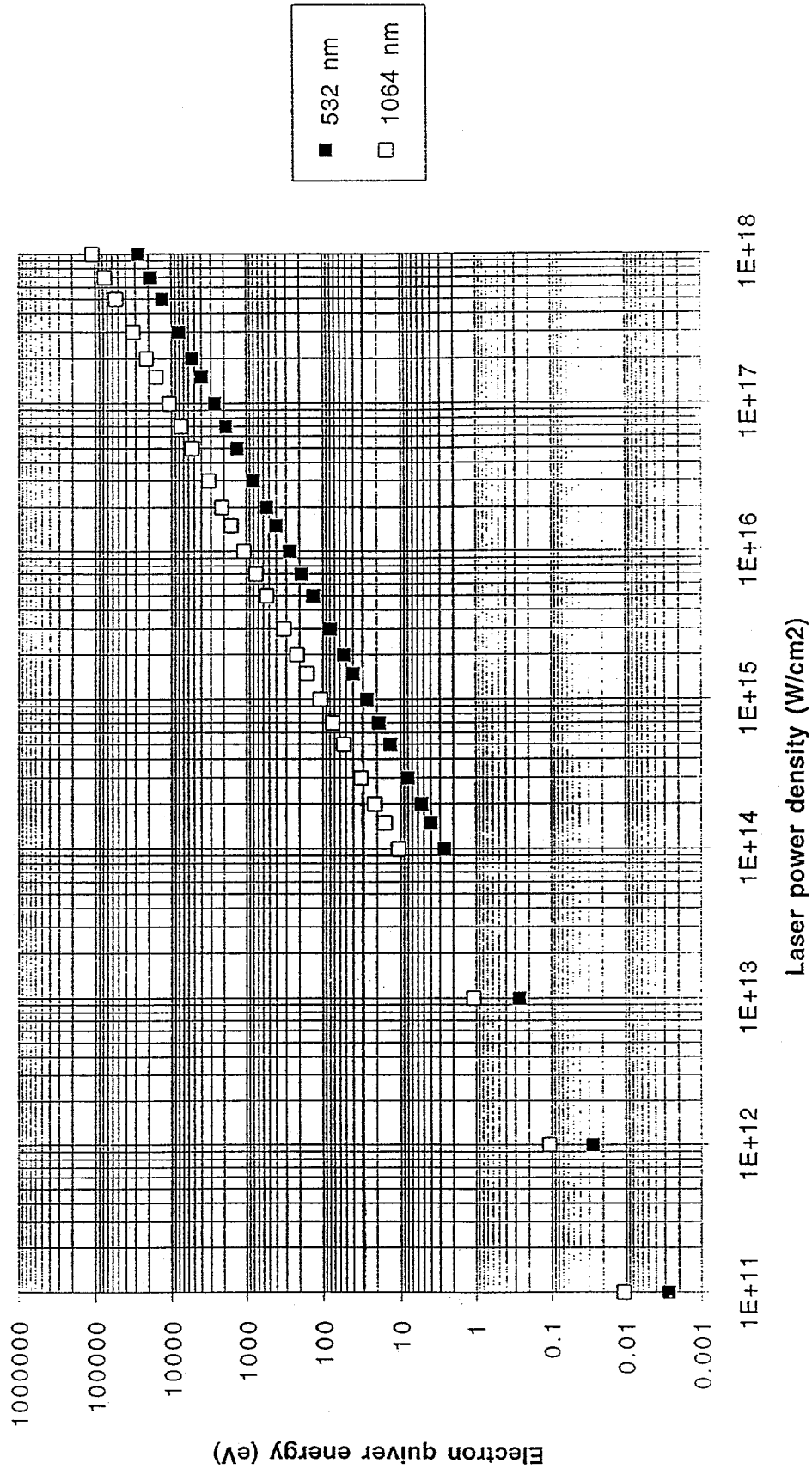


Fig. 16. Electron quiver energy as a function of laser power density for 532 and 1064 nm light.